PETROGENESIS OF MANTLE PERIDOTITES FROM THE IZU-BONIN-MARIANA (IBM) FOREARC

Alberto Zanetti*,✉, Massimo D'Antonio, Piera Spadea***, Nicola Raffone°, Riccardo Vannucci*,°** and **Olivier Bruguier°°**

* *CNR-Istituto di Geoscienze e Georisorse, Sezione di Pavia, Italy.*
** *Dipartimento di Scienze della Terra, Università Federico II, Napoli, Italy.*
*** *Dipartimento di Georisorse e Territorio, Università di Udine, Italy.*
° *Dipartimento di Scienze della Terra, Università di Pavia, Italy.*
°° *ISTEEM-CNRS, Montpellier, France.*
✉ *Corresponding author, e-mail: zanetti@crystal.unipv.it.*

Keywords: *Forearc mantle peridotite, supra-subduction zone, partial melting, porous flow reaction, Izu-Bonin-Mariana.*

ABSTRACT

Serpentinised spinel harzburgites to orthopyroxene-rich spinel dunites recovered during the Ocean Drilling Program (ODP) Leg 195 on top of the South Chamorro Seamount (southern sector of the Mariana forearc, West Pacific Ocean), along with additional spinel harzburgites from Conical and Torishima Seamounts (northern Mariana and Izu-Bonin forearc, respectively), previously collected during the ODP Leg 125, have been investigated to shed light on the nature and evolution of forearc mantle in the intra-oceanic supra-subduction environment.

All the samples show a marked heterogeneity in terms of petrographic, mineralogical and geochemical features that suggests a complex, multistage evolution involving, at variable extent, partial melting, reactive porous flow melt migration and subsolidus metamorphic re-equilibration under decreasing T and open system conditions. Geochemical evidence of the interaction between peridotites and various melts/fluids is the ubiquitous enrichment in highly incompatible elements, such as Large Ion Lithophile Elements (LILE).

As for the high-T evolution of these peridotites, a three-stages-model is proposed, involving: 1) a former depletion event, during which the IBM forearc peridotites experienced 20-25% polybaric fractional melting during adiabatic upwelling; 2) a second depletion event characterised by a marked impoverishment in modal orthopyroxene, related to the upraise migration of ultra-depleted melts; 3) a late interaction between a relatively small volume of residual melts and the refractory mantle sequence. Oxidation state of the mantle minerals meanly decreases from north (Torishima Seamount) to south (South Chamorro), according to significant different contributions coming from the subducted Pacific Plate. In particular, the absence of a marked oxidation in South Chamorro peridotites suggests that the percolating melts during Stage 2 had not significant slab-derived component.

This observation lead us to conclude that a thermal anomaly in the western Pacific mantle rather than the injection of hydrous components must be the "engine" determining the extreme depletion of the oceanic forearc peridotites and the arc formation. In this frame, it is proposed that IBM peridotites during Stage 1 underwent decompression partial melting and contributed to arc volcanism as actual mantle source. Successively, they were emplaced at relatively shallow levels (Stage 2), constituting the top of a strongly refractory mantle column and being percolated by melts produced by plumbing sources of the arc volcanism.

INTRODUCTION

Intra-oceanic Supra-Subduction Zones (SSZ) are characterised by an extreme complexity in terms of geological and tectonic environments. They can comprise trenches, volcanic arcs, spreading centres, fracture zones, mud seamounts in the forearc, backarc and forearc basins, whose spatial relationships may rapidly change with time. Consistently, mantle peridotites recovered from this realm commonly record a multistage evolution that can furnish valuable information for unravelling the petrologic and geodynamic processes underwent by different SSZ regions (e.g. Pearce et al., 2000, and references therein).

The mantle peridotites recovered from forearc regions are of particular interest to place constraints on the origin and the early evolution of SSZ. Since Bonatti and Michael (1989), it has been assessed that forearc peridotites are more refractory than abyssal peridotites far from trenches. This distinctive character was firstly interpreted as the evidence of additional partial melting episodes in mantle wedge systems due to introduction of water released by subducting slabs and possibly related to arc tholeiites and/or boninites generation. The relevance of this process was fundamentally recognised also by successive works focalised on the forearc peridotites from the Izu-Bonin-Mariana (Ishii et al., 1992; Parkinson et al., 1992; Parkinson and Pearce, 1998) and South Sandwich areas (Pearce et al., 2000).

However, the importance of the percolation of exotic melt/fluid after partial melting episodes in modifying the mineralogical, petrographic and geochemical features of these peridotites was progressively highlighted.

Pearce et al. (2000) concluded that a range of types of mantle can occur in forearc settings: MORB lithosphere interacting with arc magma (Mariana forearc), transitional lithosphere interacting with arc magma (South Sandwich forearc), slightly depleted mantle interacting with back-arc basin magma (South Sandwich Trench-Fracture Zone intersection), and arc lithosphere interacting with arc magma (Izu-Bonin forearc).

More recent hypotheses on the genesis of the SSZ magmatism (and, in particular, of boninites) and of the geological conditions allowing for the onset of intra-oceanic subduction invoke a positive thermal anomaly of the mantle related to plume upwelling and/or asthenosphere flow (Macpherson and Hall, 2001; Flower et al., 2001; Niu et al., 2003).

A new opportunity to document the petrologic features of forearc peridotites has been provided by drilling at Site 1200 during Ocean Drilling Program (ODP) Leg 195 (Shipboard Scientific Party, 2002). In this Site, the top of the

South Chamorro Seamount, located in the Mariana forearc, was cored, and several fragments of serpentinised mantle peridotites were recovered. Although the degree of serpentinisation of these samples is rather large, the occurrence of relics of the primary and secondary mineral assemblages allowed us to document a series of re-crystallisation events at high-T, mantle condition. In this paper, the major and trace element composition of bulk rock, as well as the major element mineral chemistry, of a suite of South Chamorro serpentinites will be shown, along with that of a number of peridotite samples previously recovered during the ODP Leg 125 at Conical Seamount (Site 779A; Mariana forearc) and Torishima Seamount (Site 784A; Izu-Bonin forearc), respectively (Fryer and Pearce, 1992). The data will be addressed in order to assess: 1) the extent of partial melting process; 2) the occurrence of melt-peridotite reaction and, if it is the case, the geochemical characteristics of the migrating melt(s); 3) the possible geodynamic scenarios in which these processes occurred.

TECTONIC SETTING AND GEOLOGY OF THE WEST PACIFIC OCEAN

Volcanism at the Izu-Bonin-Mariana (IBM) arc started in Oligocene, about 26 My ago, in response to subduction and hinge roll-back of the Pacific Plate along the eastern Philippine Sea Plate margin, contemporaneously to east-west backarc spreading that led to the progressive opening of the Parece-Vela and Shikoku basins to the east (Hall, 2002; Deschamps et al., 2002), which lasted until present. This tectonic setting was preceded by an early stage of rifting related to NW-SE spreading along the Central Basin Spreading Centre, which caused the opening of the West Philippine Basin, since approximately 58 until 45-42 My ago (Hilde and Lee, 1984; Hall et al., 1995; Fujioka et al, 1999; Deschamps and Lallemand, 2002). In the same period, subduction occurred several hundreds of kilometres west of the present-day position of the IBM arc, along a proto-IBM volcanic arc represented by the now submerged, Palau-Khyushu Ridge (Fig. 1).

The IBM convergent plate margin system is non-accretionary. The forearc between the trench and the arc is characterised by a chain made up of numerous, large mud volcanoes, 30 km in diameter and 2 km in height, meanly (e.g., Fryer, 1992a; 1992b; 1996; Fig. 2a). The mud volcanoes are composed mainly of unconsolidated flows of serpentine mud, which encloses clasts consisting by serpentinised mantle peridotite (Fryer, 1992b) and subordinately blueschist materials (Maekawa et al., 1995; Fryer et al., 1999; Shipboard Scientific Party, 2002). Faulting of the forearc down to depths of tens of km produces fault detritus that mixes with slab-derived fluids, generating a thick, gravitationally unstable mixture of mud and rock that rises in conduits along the fault plane to the seafloor (Fryer, 1992a; 1992b; 1996). These mud volcanoes are considered a unique geological probe of both the forearc lithosphere and the décollement region between the subducting Pacific Ocean Plate and the overlying wedge of the forearc West Philippine Sea Plate. This probe, through episodic protrusion events, provides opportunity to investigate processes and conditions at depths down to 35 km beneath the forearc (Fryer, 1992a; 1992b; 1996). Some of these seamounts (e.g. the South Chamorro Seamount and the Conical Seamount) are currently venting fluids through aragonite chimneys located on their summit. The geochemical features of these fluids suggest that they carry a component derived by dehydration processes occurring in the subducting Pacific Plate and liberating at the décollement zone (Mottl, 1992; Mottl et al., 2003).

LOCATION OF THE INVESTIGATED SERPENTINE MUD VOLCANOES

The South Chamorro, Conical and Torishima Seamounts are located at a distance of about 100 km to the west of the trenches (Figs. 1 and 2).

This is the first documentation of the mantle lithosphere composition in the South Chamorro area. The South Chamorro Seamount is located at 13°47´ N, 146°00´ E, about 125 km east of Guam Island (Fig. 2), and was drilled by ODP during Leg 195 (Shipboard Scientific Party, 2002). It lies 85 km west of the trench, where the downgoing slab is ca. 26.5 km deep. This seamount is a partly collapsed, roughly conical, edifice ca. 2 km high and 20 km wide with active serpentine/blueschist mud volcanism (Shipboard Scientific Party, 2002).

Both Conical and Torishima Seamounts were drilled by ODP during the Leg 125 (Fryer, 1992b). The Conical Seamount is located at 19°35´ N, 146°40´ E, about 80 km west of the Mariana trench axis, and at about 30 km above the subducting Pacific plate. It is a cone-shaped, 1500 m high edifice, with a diameter of 20 km (Fryer, 1992b). The Torishima Seamount, 1400 m high and 20 km in diameter, is located at 30°55´ N, 141°47´ E, 30 km east of the Bonin trench axis, lying 20 km above the subducting Pacific Plate.

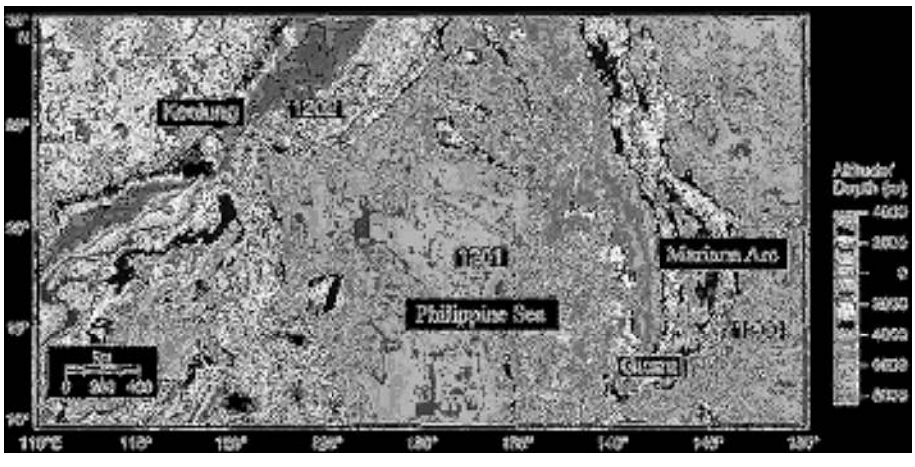

Fig. 1 - Location of Sites drilled during Ocean Drilling Program Leg 195 in the Mariana system.

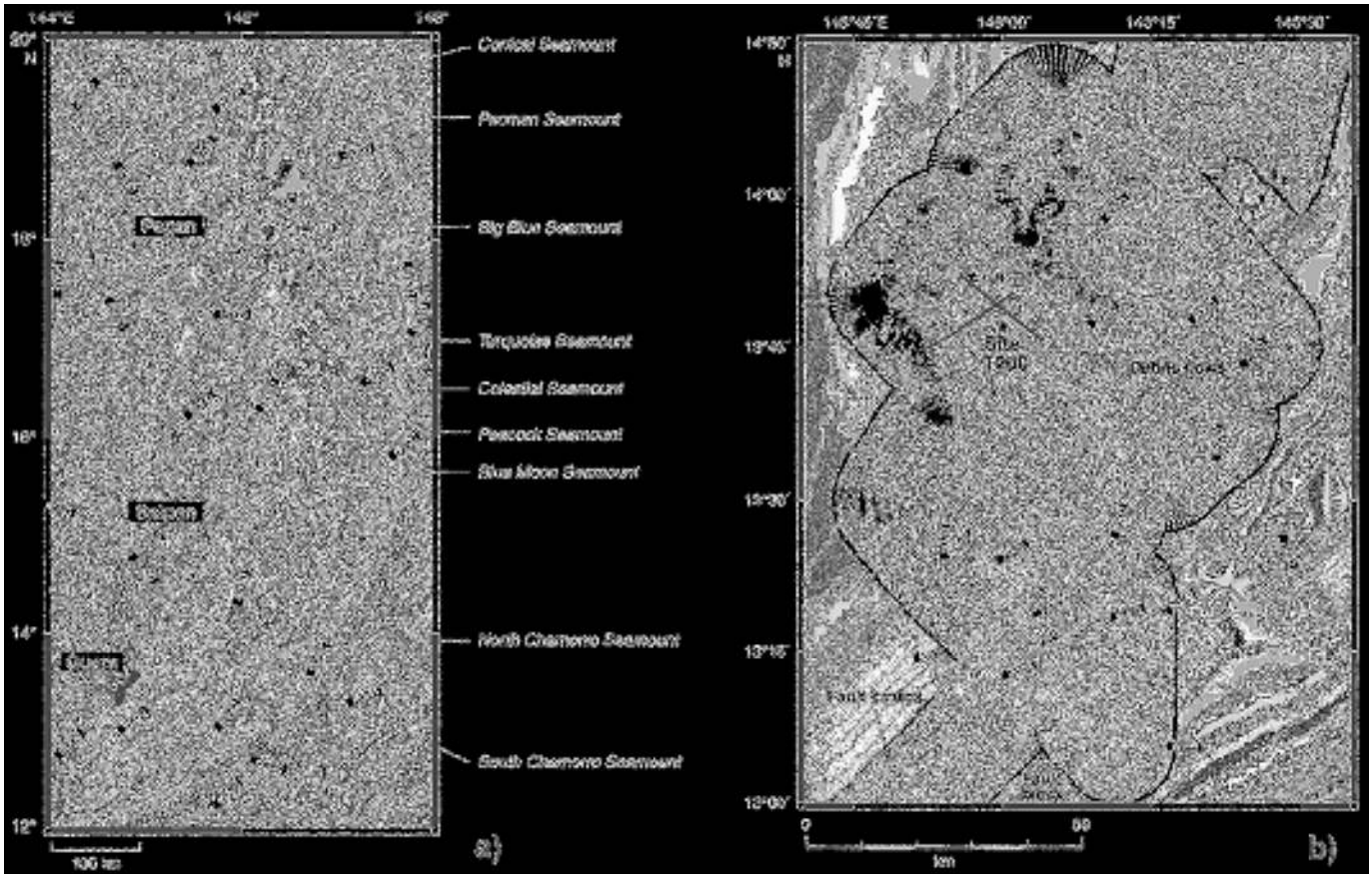

Fig. 2 - a) The bathymetry of the south-eastern part of the Mariana system from 12°N to 20°N, showing the chain of serpentine mud volcanoes resting on the forearc. Contour interval is 200 m. Serpentine and blueschist mud volcanoes of Mariana forearc that have been sampled are labelled. b) Shaded, contoured bathymetry of the region included between North and South Chamorro Seamounts.

In contrast to the South Chamorro and Conical Seamounts, it is draped by a thicker (ca. 1 km vs. a few tens of meters) sedimentary sequence constituted by serpentinite mud, as shown by drilling. The petrochemical features of ultramafic fragments from these two mud volcanoes were addressed by Ishii et al. (1992), Parkinson et al. (1992) and Parkinson and Pearce (1998).

SAMPLE SELECTION AND PETROGRAPHIC FEATURES

Peridotite fragments recovered at South Chamorro Seamount are deeply serpentinised, mostly spinel harzburgites and minor dunites. Most olivine is transformed in mesh-textured serpentine + brucite + magnetite, whereas orthopyroxene is frequently replaced by bastite serpentine + magnetite. Serpentine minerals are mostly lizardite and chrysotile with variable Al_2O_3 and Cr_2O_3 contents, whereas brucite has a variable, often high Fe(OH) content, up to 40% (D'Antonio and Kristensen, 2004). Relatively fresh areas with relics of mantle minerals can be found in most of the samples. These zones ubiquitously show strongly deformed porphyroclastic textures, which bring evidence for a complex evolution characterised by several recrystallisation events. These latter are recorded by the growth of different mineral assemblages. As a rule, the grain size of the secondary, recrystallised minerals becomes finer in the later assemblages. The modal mantle composition (Table 1) has been estimated by: i) least-square fitting of the major element chemistry of mineral and bulk rock; ii) petrographic observation. The latter method can ensure valuable assessment of the olivine and orthopyroxene modal ratio also in so deeply serpentinised samples due to the widespread occurrence of "ghosts" of the peculiar mineral structure, such as the exsolution lamellae of orthopyroxenes. The primary assemblage is represented by large porphyroclasts of olivine, orthopyroxene and spinel (Mineral Assemblage I). Clinopyroxene modal content is between 3% to null. The occurrence of primary clinopyroxene (Cpx I) is doubtful and limited to very few samples (e.g. harzburgite 195 1200A 6R1, 93-96 cm), in which relatively large (0.5 mm), exsolved and slightly cloudy clinopyroxenes show sharp boundaries with the primary orthopyroxene. The olivine porphyroclasts are kinked, elongated, and parallel to each other, along the main foliation plane. Such a foliation is also highlighted by chains of elongated and fragmented spinels. Primary orthopyroxenes are curved, sometimes broken. They are strongly exsolved and frequently enclose subhedral to prismatic clinopyroxene grains (Cpx II), which modally increase towards the rim. Such secondary clinopyroxenes have been interpreted as the result of the interaction of the peridotite with percolating melts, rather than the metamorphic exsolution from an original Ca-richer orthopyroxene composition (Parkinson and Pearce, 1998, and references therein). A melt-related origin can be argued also for the curvilinear embayments characterising the rim of the orthopyroxene porphyroclasts, where they are replaced by secondary fine-grained mineral assemblage formed by anhedral to subhedral olivine II + orthopyroxene II ± clinopyroxene II. These

Table 1. Whole rock major and trace element composition of the serpentinised peridotites from Izu-Bonin-Mariana forearc.

	SOUTH CHAMORRO																CONRAD				BOSCHERAS	
LBO	109	105	109	105	105	105	101	103	105	105	105	105	109	105	105	105	105	105	125	125	125	125	121	125
Hole	1209A	1209A	1209A	1209A	1209A	1209A	1209A	1209A	1209A	1209A	1209A	1209A	1209B	1209A	1209A	1209A	1209A	1209A	779A	779A	779A	779A	784A	784A
Core	30R1	5R1	6R1	6R2	7R2	10R1	10R1	11R1	14R1	16R1	19R1	19R1	1R1	16R1	16R1	16R2	1R1	1R1	22R1	26R2	36R1	46R1C	46R1	
Interval	48-52	88-91	93-96	66-69	61-67	42-45	99-95	144-44	59-61	22-24	12-15	106-109	56-59	59-61	116-119	1-4	30-36	133-136	13-16	80-83	28-24	98-100	16-13	186-185
rock type	harz (3)	harz (3)	harz (3)	dun (3)	harz (3)	dun (3)	harz (3)	harz (3)	harz (3)	harz (3)	harz (3)	harz (3)	dun (3)	harz (3)	harz (3)	harz (3)	harz (3)	harz (3)	harz (3)	harz (3)	harz (3)	harz (3)	harz (3)	harz (3)
SiO_2 (wt%)	42.23	43.54	42.71	42.48	42.96	41.06	43.63	43.28	45.13	42.28	43.96	43.84	42.99	43.95	42.97	44.40	43.78	43.96	44.77	43.45	43.48	44.65	42.67	42.96
TiO_2	0.00	0.00	0.01	0.02	0.00	0.00	0.00	0.01	0.01	0.00	0.00	0.01	0.00	0.00	0.00	0.00	0.00	0.01	0.01	0.01	0.01	0.01	0.01	0.01
Al_2O_3	0.46	0.69	0.68	0.80	0.65	0.55	1.06	0.65	0.71	0.74	0.78	0.71	0.98	0.44	0.34	0.92	0.66	0.79	0.76	0.58	0.56	0.98	0.72	0.75
Fe_2O_3	8.65	8.90	8.53	8.99	8.65	8.92	8.46	8.64	8.53	8.74	8.58	8.60	8.68	8.85	8.73	8.42	8.77	8.36	8.55	8.41	8.50	8.89	8.65	8.34
MnO	0.13	0.13	0.13	0.13	0.12	0.12	0.12	0.12	0.12	0.13	0.12	0.13	0.12	0.11	0.11	0.13	0.12	0.13	0.13	0.13	0.13	0.13	0.13	0.13
MgO	47.21	45.68	46.21	46.68	45.99	48.43	44.28	45.80	45.87	47.48	44.96	44.83	46.36	47.30	46.34	44.50	45.35	44.95	44.34	46.44	43.99	47.62	45.82	44.89
CaO	0.44	0.50	0.48	0.68	0.68	0.31	1.16	0.52	0.70	0.58	0.70	0.76	0.42	0.29	0.80	0.93	0.87	0.74	0.70	0.35	1.30	1.16	0.80	0.71
Na_2O	0.07	0.15	0.14	0.11	0.12	0.15	0.19	0.14	0.14	0.16	0.14	0.17	0.14	0.13	0.15	0.17	0.14	0.16	0.20	0.11	0.14	0.06	0.15	0.14
K_2O	0.01	0.01	0.04	0.04	0.04	0.04	0.05	0.05	0.04	0.04	0.05	0.05	0.04	0.04	0.04	0.05	0.05	0.05	0.05	0.04	0.03	0.03	0.02	0.02
P_2O_5	0.00	0.00	0.00	0.01	0.00	0.00	0.00	0.01	0.01	0.00	0.00	0.01	0.01	0.01	0.00	0.01	0.01	0.01	0.01	0.01	0.01	0.01	0.01	0.01
Tot	99.34	99.25	99.13	100.10	99.21	99.27	99.15	99.23	100.45	100.27	99.26	99.23	99.17	99.45	99.29	99.45	98.68	99.15	99.51	99.43	98.74	98.76	97.06	96.85
Mg#	0.92	0.91	0.91	0.92	0.91	0.92	0.91	0.91	0.92	0.93	0.91	0.91	0.91	0.91	0.91	0.91	0.91	0.91	0.91	0.92	0.91	0.91	0.91	0.91
LOI (wt%)	12.90	14.61	14.65	13.73	13.62	15.56	15.29	13.63	13.84	14.55	11.38	14.29	14.13	13.25	16.35	13.05	14.05	13.31	13.64	14.32	9.89	9.56	13.54	12.30
Serp (%)	92	84	88	74	78	92	68	76	77	81	63	79	79	99	96	68	78	74	72	57	48	52	85	68
Sc (ppm)		8	6		8	4	10	6	7	7	9	7	6							5	10	10	6	7
V		25	27		14	13	39	23	35	32	39	26	31							12	45	47	18	25
Cr		1811	2146		1974	1768	2681	1990	1943	2357	2918	2270	2184							622	2127	1998	858	1980
Co		98	102		103	109	92	101	100	98	99	102	99							96	95	90	97	94
Ni		2102	2156		2093	2261	1992	2141	2060	2130	2084	2068	2073							2029	2101	2127	2178	2121
Cu		4.8	8.8		6.2	4.0	4.2	4.8	4.4	8.4	2.4	2.4	4.6							9.0	18	13	6.8	12
Zn		46	37		36	48	41	37	46	50	44	39	35							48	46	66	70	59
Ga		0.71	0.90		0.35	0.56	0.29	0.43	0.40	0.38	0.35	0.35	0.35							b.d.l.	b.d.l.	b.d.l.	b.d.l.	b.d.l.
Ge		0.49	0.53		0.52	0.56	0.78	0.49	0.53	0.62	0.61	0.63	0.59							0.56	1.0	1.1	0.67	0.76
As		1.3	0.95		0.95	0.85	1.3	1.1	1.4	0.98	1.6	1.3	0.93							0.97	0.79	0.40	0.851	0.80
Sr		14	6.8		11	7.3	34	13	17	14	13	17	7.5							2.8	4.6	5.3	5.8	5.6
Y		0.014	0.013		0.015	0.026	0.14	0.017	0.53	0.016	0.028	0.33	0.044							0.036	0.14	0.13	0.036	0.031
Zr		0.048	0.043		0.041	0.042	0.045	0.052	0.055	0.036	0.037	0.12	0.17							0.21	0.27	0.11	0.040	0.045
Nb		0.051	0.052		0.019	0.049	0.019	0.017	0.024	0.023	0.11	0.21	0.029							0.020	0.028	0.025	0.012	0.016
Mo		0.097	0.054		0.10	0.11	0.12	0.094	0.083	0.085	0.12	0.094	0.15							0.36	0.35	0.13	0.19	0.47
Li		1.1	2.3		1.7	1.7	1.0	9.3	7.5	2.4	2.3	2.6	1.3							1.2	2.4	2.6	1.6	2.3
Be		0.070	0.070		0.070	0.070	0.070	0.070	0.088	0.070	0.080	0.080	0.070							0.26	0.26	0.26	0.15	0.15
Cs		1.2	0.37		0.28	0.17	0.83	0.48	0.91	0.30	0.43	0.33	0.48							0.33	0.05	0.09	0.17	0.29
Ba		2.3	3.6		1.7	1.8	5.2	2.9	2.5	3.2	6.5	2.8	2.8							2.2	3.7	3.3	0.77	10
La		0.017	0.026		0.015	0.009	0.015	0.018	0.026	0.026	0.033	0.012	0.046							0.005	0.15	0.015	0.005	0.008
Ce		0.030	0.048		0.025	0.01	0.026	0.045	0.052	0.027	0.049	0.033	0.077							0.009	0.25	0.027	0.0072	0.0123
Pr		0.004	0.006		0.003	0.006	0.003	0.003	0.004	0.003	0.006	0.006	0.010							0.0014	0.036	0.009	0.0015	0.0017
Nd		0.013	0.015		0.010	0.019	0.013	0.013	0.019	0.013	0.030	0.021	0.050							0.0073	0.089	0.026	0.0028	0.0050
Sm		0.003	0.005		0.003	0.005	0.006	0.004	0.005	0.003	0.007	0.007	0.012							0.0022	0.019	0.0090	0.0012	0.0020
Eu		0.001	0.002		0.001	0.002	0.001	0.001	0.002	0.001	0.003	0.003	0.003							0.0006	0.0055	0.0022	0.0004	0.0002
Gd		0.003	0.003		0.004	0.005	0.006	0.003	0.003	0.002	0.004	0.005	0.008							0.0043	0.015	0.0050	0.0008	
Tb		0.001	0.001		0.001	0.001	0.002	0.001	0.001		0.001	0.002	0.002							0.0007	0.0018	0.0010	0.0002	0.0005
Dy		0.004	0.003		0.005	0.007	0.021	0.004	0.006	0.004	0.006	0.024	0.030							0.0044	0.020	0.006	0.0020	0.0048
Ho		0.001	0.001		0.001	0.001	0.007	0.002	0.002	0.001	0.001	0.005	0.006							0.0015	0.006	0.0045	0.0005	0.0015
Er		0.003	0.003		0.005	0.006	0.025	0.007	0.008	0.006	0.006	0.019	0.018							0.0051	0.022	0.009	0.0017	0.0050
Tm		0.001	0.000		0.002	0.001	0.006	0.001	0.002	0.001	0.001	0.003	0.003							0.0010	0.0045	0.0042	0.0004	0.0012
Yb		0.010	0.006		0.013	0.007	0.040	0.013	0.017	0.013	0.015	0.025	0.020							0.0069	0.038	0.026	0.0032	0.0118
Lu		0.001	0.001		0.002	0.001	0.006	0.002	0.003	0.002	0.002	0.004	0.003							0.0012	0.0063	0.0043	0.0009	0.0018
Hf		0.002	0.002		0.007	0.004	0.007	0.004	0.006	0.004	0.005	0.008	0.006							0.0090	0.010	0.005	0.0020	0.0051
Ta		0.020	0.013		0.012	0.002	0.002	0.004	0.002	0.002	0.002	0.002	0.002							0.0014	0.006	0.005	0.0021	0.0013
Tl		0.004	0.002		0.003	0.000	0.006	0.003	0.004	0.002	0.002	0.003	0.002							0.0015	0.004	0.006	0.0015	0.0014
Pb		0.28	0.16		0.60	0.34	0.22	0.24	0.26	0.24	0.28	0.22	0.28							0.13	0.14	0.22	0.13	0.24
Th		0.005	0.002		0.002	0.000	0.002	0.003	0.004	0.002	0.002	0.003	0.002							0.0016	0.010	0.012	0.0014	0.0019
U		0.002	0.002		0.002	0.000	0.003	0.002	0.002	0.002	0.002	0.003	0.002							0.0010	0.021	0.006	0.0008	0.0009
Ol	86.3	79.7	80.8	81.6	79.5	90.8	72.0	79.3		85.4	72.5	74.6	88.7	96.0	94.2	78.3	88.9	85.5	84.8	78.1	68.1	94.4	78.5	73.6
Opx	12.4	23.8	20.6	16.5	18.5	8.2	25.5	19.9		10.5	24.3	22.3	10.4	3.2	12.0	20.0	10.0	13.0	13.0	21.1	26.6	3.7	18.8	24.0
Cpx	1.3	5.8	2.0	1.8	1.1	0.6	2.5	1.5		2.2	1.9	2.4	1.1	0.8	3.0	1.0	1.0	2.5	tr	0.8	4.3	1.8	1.9	2.1
Sp	0.3	5.5	0.6	2.1	0.9	0.4	0.4	1.2		1.8	1.3	0.7	0.8	0.6	5.8	0.7	0.1	1.0	2.2	0.3	1.0	0.1	0.7	0.3

Modes are in weight percent and have been estimated based on (1) least-square fitting method using the whole-rock and the mineral chemistry and (2) point counting. (3) No thin section available. LOI = Loss On Ignition. Serp = Serpentinisation. See text for more explanation

secondary phases also fill the interstices among the large porphyroclasts, in association with secondary spinel (Mineral Assemblage II). Both pyroxenes of this interstitial assemblage show exsolution lamellae. The largest secondary spinels occur in symplectitic textures along with pyroxenes and olivine. The late crystallisation stage of the Mineral Assemblage II is characterised by finer, exsolution-free, orthopyroxenes and clinopyroxenes, associated with spinel. The clinopyroxene occurring in fine-grained zones shows vermicular shapes and probably filled the last interstices. The spinel grains are anhedral to perfectly euhedral.

Amphibole is rather rare, and mostly occurs as coronas around clinopyroxene. Nevertheless, amphibole pseudoveins in equilibrium with the secondary assemblage have been observed in the harzburgite 195 1200A 3R1, 49 cm. The occurrence of amphiboles in IBM forearc peridotites has been previously described by Ohara and Ishii (1998) and Parkinson and Pearce (1998).

Samples from Conical Seamount (Leg 125 Site 779) are spinel harzburgites. Samples 125 779A 26R2, 20-24 cm and 125 779A 26R2, 98-100 cm have a porphyroclastic texture similar to that described for South Chamorro Seamount serpentinites. They show a relatively large clinopyroxene modal content (1.8-4.3% by volume). In contrast, the harzburgite sample 125 779A 22R1, 60-68 cm preserves a protogranular texture characterised by coarse-grained olivine and spinel. In this sample, clinopyroxene occurs in form of very small grains (~100 μm long) locally concentrated along the rim of large orthopyroxenes: it is likely related to a very late crystallisation stage.

Samples from Torishima Forearc Seamount (Leg 125 Site 784) are spinel harzburgites with a strongly deformed porphyroclastic texture. They are largely serpentinised. Spinel, up to 1 mm wide, is strained and lies mainly along trails, highlighting structural lineation. Clinopyroxene is relatively abundant (2% by volume), occurring either in the interstices or within orthopyroxene porphyroclasts. The interstitial clinopyroxene is anhedral and about 800-900 μm in length. The clinopyroxene within orthopyroxene is prismatic to round and smaller (< 400 μm). Both types of clinopyroxene show thin exsolution lamellae.

ANALYTICAL TECHNIQUES

Bulk rock XRF analyses were carried out with the PW 2400 spectrometer at the Dipartimento di Mineralogia e Petrologia, Padova University, for 19 samples from South Chamorro Seamount, 3 samples from Conical Seamount and 2 samples from Torishima Seamount. Major elements were measured on lithium borate glass discs prepared with a flux to sample ratio of 10:1 to reduce matrix effects. Loss on ignition was determined by gravimetric method. Bulk rock trace element analyses of 11 South Chamorro serpentinites (Rare Earth Elements, Sc, V, Cr, Co, Ni, Cu, Zn, Sn, Ga, Rb, Sr, Y, Zr, Nb, Mo, Li, Be, Cs, Ba, Hf, Ta, Tl, Pb, Th, U) were carried out by inductively-coupled plasma-mass spectrometry (ICP-MS) at the Centro de Instrumentaciòn Cientifica, Granada University. Sample preparation involved digestion of 0.1 g of sample in HNO_3 + HF at high pressure and temperature, evaporation to dryness, and subsequent dissolution in 100 ml of 4 vol.% HNO_3. Measurements were carried out in triplicate with a PE SCIEX ELAN-5000 spectrometer, with Re and Rh used as internal standards. Precision (2σ) was about ± 3 rel.% and ± 8 rel.% for concentrations of 50 and 5 ppm, respectively. Trace element analyses on whole rock of the Conical and Torishima Seamounts samples were performed by conventional nebulization ICP-MS using a VG Plasmaquad II turbo (+ "Option S") housed at the University of Montpellier II. Rock digestion on 100 mg of sample followed the procedure outlined in Ionov et al. (1992). Whole rocks were dissolved twice on a hot plate at 150°C with a mixing of 48% HF/$HClO_4$ for 48 hours in closed teflon beakers. After evaporation all samples were subjected to three steps of evaporation with decreasing $HClO_4$ quantities and at increasing temperatures up to 180°C to remove fluorides. Samples were then dissolved in 2% HNO_3 and diluted shortly before analysis to a final dilution factor ranging from 1000 to 2000, resulting in a total dissolved solid of 0.1 to 0.05%. Dilution factors were kept high to minimise drift which was corrected by addition of doping elements, namely In and Bi, at a concentration level of 10 ppb. REE, HFSE (Nb, Ta, Zr, Hf) and LILE (Cs, Rb, Ba, Th, U and Sr) were analysed. Concentrations were determined by external calibrations except for Nb and Ta which were measured by surrogate calibration using Zr and Hf respectively following the method outlined by Jochum et al. (1986) for Spark Source Mass Spectrometry and applied to ICP-MS in this study. Reproducibility and accuracy were checked by carrying out replicate analyses of both certified reference materials (BEN, UBN and PCC1) and samples. Polyatomic interferences were controlled by running the machine at an oxide production level < 1% and corrected by running batches of synthetic solutions containing interfering elements.

Minerals were analysed on the WDS Camebax SX50 Cameca equipment at the CNR-Istituto di Geoscienze e Georisorse, Sede di Padova. Operating conditions were 15 kV accelerating voltage and 2.2 nA beam current. Synthetic and natural standards were used for calibration and quantification procedures.

COMPOSITIONAL FEATURES

Major and trace element bulk-rock chemistry

The major and trace element composition of peridotites from South Chamorro Seamount (volatile-free basis) are shown in Table 1. They possess high Mg# values [0.911-0.916: expressed as molar $Mg/(Mg + Fe_T)$] and low to very low contents in fusible elements such as Al_2O_3 (0.33-1.06 wt%), CaO (0.29-1.14 wt%) and TiO_2 (≤ 0.02 wt%). SiO_2 is variable, but reaches a very low value (41.9 wt%), and is correlated negatively with MgO (Fig. 3). This latter is in the range of 44.3-48.4 wt%. The loss on ignition (LOI) value is in the range of 11.0-17.8 wt% (Fig. 4), that corresponds to an estimated degree of serpentinisation [expressed as 100 x $LOI/PM(H_2O)$] between 61 and 99%. As a whole, the compositional range of the South Chamorro peridotites overlaps that defined by the most depleted abyssal peridotites reported by Niu (1997) and Baker and Beckett (1999). The peridotites from the Conical and Torishima Seamounts analysed in this work (Table 1) also show highly refractory bulk-rock compositions within the compositional field defined by the data of Parkinson and Pearce (1998) (Fig. 4). The Conical harzburgites have LOI values between 8.7 and 10.3 wt% (estimated serpentinisation degree 52-57%), lower than those of the South Chamorro peridotites. The harzburgites from Torishima Seamount have LOI = 12.2-15.2 wt% (estimated serpentinisation degree in the 68-82% range), indicat-

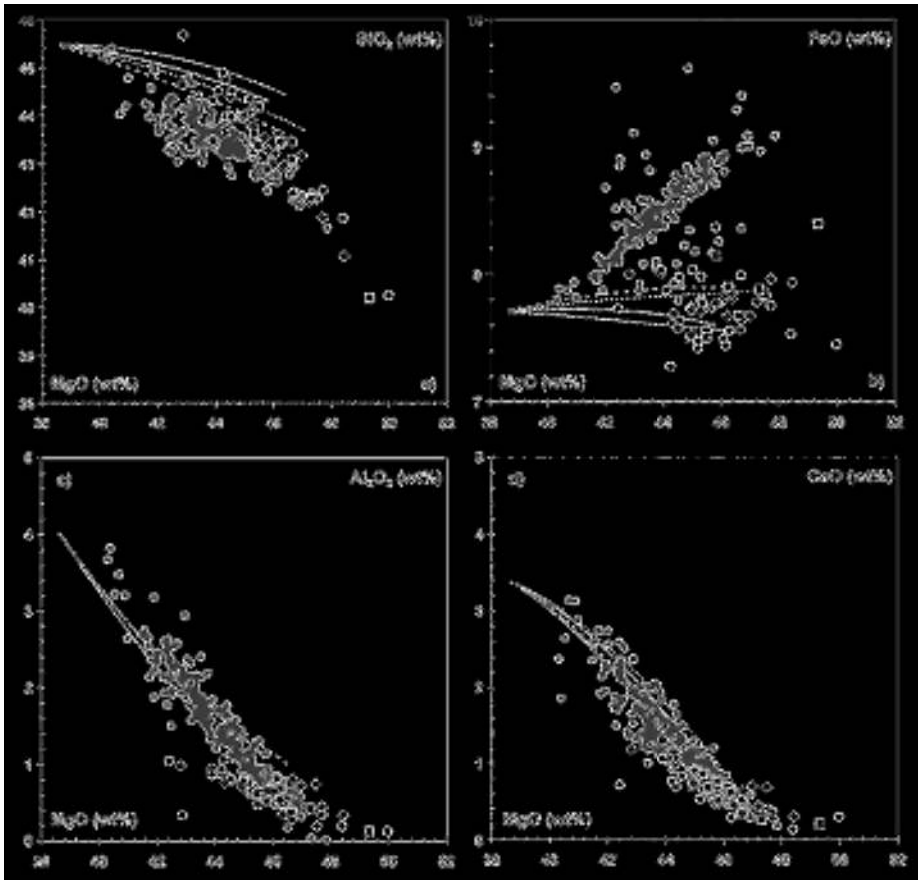

Fig. 3 - Bulk rock MgO (wt%) vs. SiO_2 (wt%), FeO (wt%), Al_2O_3 (wt%) and CaO (wt%) diagrams of the analyzed peridotites from Conical (filled circles), Torishima (filled squares) and South Chamorro (filled rhombuses) Seamounts. Empty circles and squares are the composition of peridotites from Conical and Torishima Seamounts, respectively, reported by Parkinson & Pearce (1998). Grey circles are the composition of abyssal peridotites (Niu, 1997). Melting trends calculated by Niu (1997) are reported for comparison. Legend: thin dashed and continuos lines are trends related to polybaric fractional melting in the range of 1.5-0.8 GPa and 2.5-0.8 GPa, respectively; heavy dashed and continuos lines are the trends related to batch melting at constant P, i.e. 1 and 2 GPa, respectively.

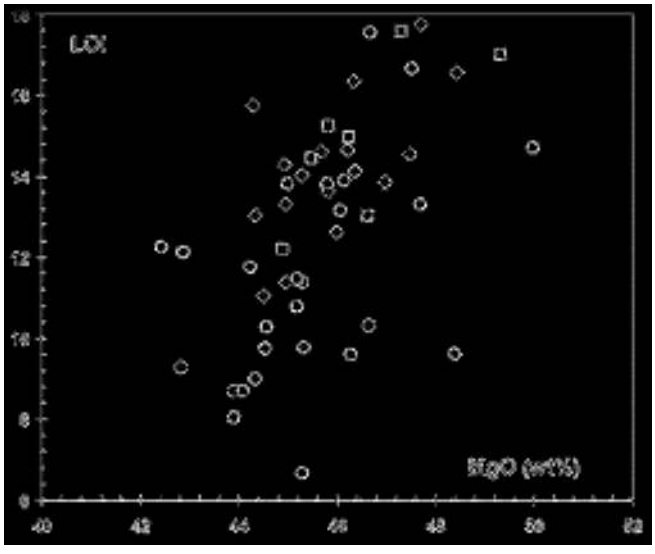

Fig. 4 - Variation diagram of loss on ignition LOI (wt%) vs. MgO (wt%) contents in peridotites from Conical (filled circles), Torishima (filled squares) and South Chamorro (filled rhombuses) Seamounts. The composition of peridotites (Conical Seamount: empty circles; Torishima Seamount: empty squares) studied by Parkinson and Pearce (1998) are reported for comparison.

ing that they have experienced low-temperature alteration to a greater extent than the peridotites from the other seamounts. As expected from the major oxides data, the South Chamorro peridotites have very low absolute concentration in incompatible trace elements. Their bulk rock C1-normalised REE patterns (Fig. 5; C1 values from Anders and Grevesse, 1989) are convex-downward, with La_N/Sm_N = 1.1-11.7, Sm_N/Yb_N = 0.1-0.9 and Yb_N = 0.25-0.04. The convex-downward shape is even clearer in the multi-element spider-diagrams, due to the significant enrichment of highly-incompatible LILE and HFSE over LREE. Furthermore, the multi-element patterns are characterised by positive anomaly of Li, Sr, Ba, Cs and Ta, and high Ta_N/Nb_N and U_N/Th_N values (Fig. 6).

Similar trace element fractionation is shown by the harzburgites from Torishima and Conical Seamounts. In particular, the trace element bulk-rock composition of the Torishima harzburgites are very similar to those (amphibole-free) previously reported by Parkinson and Pearce (1998), except for the absence in our patterns of positive Eu anomaly. Porphyroclastic peridotites from Conical Seamounts show significantly higher content in REE, Sc, V and Cr than the protogranular one, whereas no systematic difference is displayed for Sr, Pb and trace elements more incompatible than La. The variation of M-HREE and other moderately incompatible elements cover the entire range defined by the Conical harzburgites documented by Parkinson and Pearce (1998). The 125 779A 26R2, 20-24 cm sample is more enriched in highly incompatible elements than that previously found in Conical harzburgites by Parkinson and Pearce (1998).

Major element mineral chemistry

Consistently with the bulk rock data, the major element chemistry of the relics of mantle minerals from the South Chamorro peridotites (Table 2) reveals an exceptional refractory character. Olivines show Fo content [100 x $Mg/(Mg + Fe_T)$ molar] in the range of 91.0-92.6 (Fig. 7a), whereas the Mg# value is in the range of 0.901-0.924 for the orthopyroxene, 0.922-0.956 for the clinopyroxene, and 0.403-0.604 for the spinel. Orthopyroxene and clinopyroxene are depleted to extremely depleted in FeO, Al_2O_3, TiO_2

Table 2. Major element mineral chemistry of representative samples.

	SOUTH CHAMORRO					CONICAL			TORISHIMA	
sample	195	195	195	195	195	125	125	125	125	125
sample	1200A	1200A	1200A	1200A	1200A	779A	779A	779A	784A	784A
sample	116R1	16R2	16R2	17G1	17G2	22R1	26R2	26R2	45RCC	45R1
sample	116-119	1-4	32-35	103-106	13-16	60-62	20-24	98-100	10-13	108-110
rock type	*harz (2)*	*harz (2)*	*harz (2)*	*harz (2)*	*harz (2)*	*harz (2)*	*harz (2)*	*harz (2)*	*harz (2)*	*harz (2)*
SiO_2 (wt%)	42.97	44.40	43.78	43.96	44.77	43.45	43.48	44.65	42.87	43.96
TiO_2	0.00	0.00	0.00	0.01	0.01	0.01	0.01	0.01	0.01	0.01
Al_2O_3	0.34	0.82	0.66	0.79	0.76	0.28	0.94	0.98	0.52	0.75
Fe_2O_3	8.73	8.42	8.57	8.36	8.55	8.41	8.90	8.89	9.05	8.34
MnO	0.12	0.13	0.12	0.12	0.13	0.12	0.13	0.13	0.13	0.12
MgO	46.34	44.50	45.28	44.95	44.34	46.64	43.90	42.82	45.82	44.89
CaO	0.69	0.93	0.87	0.74	0.79	0.35	1.30	1.18	0.60	0.71
Na_2O	0.15	0.17	0.14	0.16	0.20	0.12	0.04	0.06	0.05	0.04
K_2O	0.04	0.05	0.03	0.03	0.05	0.04	0.03	0.03	0.02	0.02
P_2O_5	0.00	0.01	0.01	0.01	0.01	0.01	0.01	0.01	0.01	0.01
Tot	99.29	99.43	99.48	99.15	99.52	99.43	98.74	98.76	99.08	98.85
#dg#	0.91	0.91	0.91	0.91	0.91	0.92	0.91	0.91	0.91	0.91
LOI (wt%)	16.35	11.05	14.03	13.31	13.04	10.32	8.69	9.28	15.24	12.20
Serp (%)	91	61	78	74	72	57	48	52	85	68
Sc						5	10	10	6	7
V						12	40	41	18	25
Cr						622	2127	1959	859	1993
Co						96	99	98	97	94
Ni						2229	2161	2127	2170	2121
Cu						9.0	18	13	6.8	12
Zn						48	40	66	70	59
Sn						b.d.l.	b.d.l.	b.d.l.	b.d.l.	b.d.l.
Ga						0.56	1.0	1.1	0.67	0.76
Rb						0.97	0.39	0.40	0.051	0.10
Sr						2.8	4.6	5.3	5.8	5.6
Y						0.036	0.14	0.13	0.036	0.031
Zr						0.21	0.27	0.11	0.040	0.068
Nb						0.029	0.038	0.023	0.012	0.018
Mo						0.56	0.55	0.18	0.19	0.47
Li						12	2.4	2.6	1.6	2.2
Be						0.16	0.16	0.16	0.15	0.15
Cs						0.33	0.05	0.10	0.17	0.59
Ba						2.2	3.7	3.3	0.77	22
La						0.005	0.15	0.035	0.005	0.008
Ce						0.0091	0.25	0.077	0.0072	0.0123
Pr						0.0014	0.026	0.009	0.0013	0.0017
Nd						0.0070	0.089	0.036	0.0069	0.0060
Sm						0.0022	0.019	0.0090	0.0022	0.0009
Eu						0.0008	0.0056	0.0022	0.0008	0.0002
Gd						0.0030	0.013	0.0082	0.0028	
Tb						0.0007	0.0024	0.0016	0.0006	0.0003
Dy						0.0061	0.020	0.016	0.0059	0.0048
Ho						0.0015	0.006	0.0045	0.0016	0.0013
Er						0.0053	0.022	0.019	0.0057	0.0056
Tm						0.0010	0.0045	0.0042	0.0014	0.0012
Yb						0.0090	0.038	0.036	0.0132	0.0121
Lu						0.0022	0.0083	0.0083	0.0029	0.0028
Hf						0.0070	0.010	0.005	0.0020	0.0021
Ta						0.0024	0.006	0.005	0.0021	0.0030
Tl						0.013	0.014	0.016	0.015	0.014
Pb						0.13	0.14	0.22	0.13	0.34
Th						0.0014	0.110	0.012	0.0014	0.0019
U						0.0010	0.021	0.006	0.0008	0.0009
Ol	84.2	78.3	88.9	80.5	84.8	78.1	68.1	64.4	78.6	73.6
Opx	12.0	20.0	10.0	18.0	15.0	21.1	26.6	33.7	18.8	24.0
Cpx	3.0	1.0	1.0	0.5	*tr*	0.8	4.3	1.8	1.9	2.1
Sp	0.8	0.7	0.1	1.0	0.2	0.1	1.0	0.1	0.7	0.3

and Cr_2O_3 with respect to abyssal peridotites (Fig. 7b and 8). In particular, Al_2O_3 (mean value) is in the range of 0.4-2.9 wt% and 0.7-3.2 wt% in orthopyroxene and clinopyroxene, respectively. Na_2O in clinopyroxene is usually lower than 0.1 wt%, with the exception of three harzburgites (samples 195 1200A 17G1, 106-109 cm, 195 1200A 6R1, 93-96 cm, and 195 1200A 6R2, 66-69 cm) and one dunite (sample 195 1200A 10R1, 42-45 cm), in which it varies between 0.3 and 0.6 wt%. CaO is particularly high in clinopyroxene, being mostly in the range of 23.4-26.1 wt%. Significantly lower

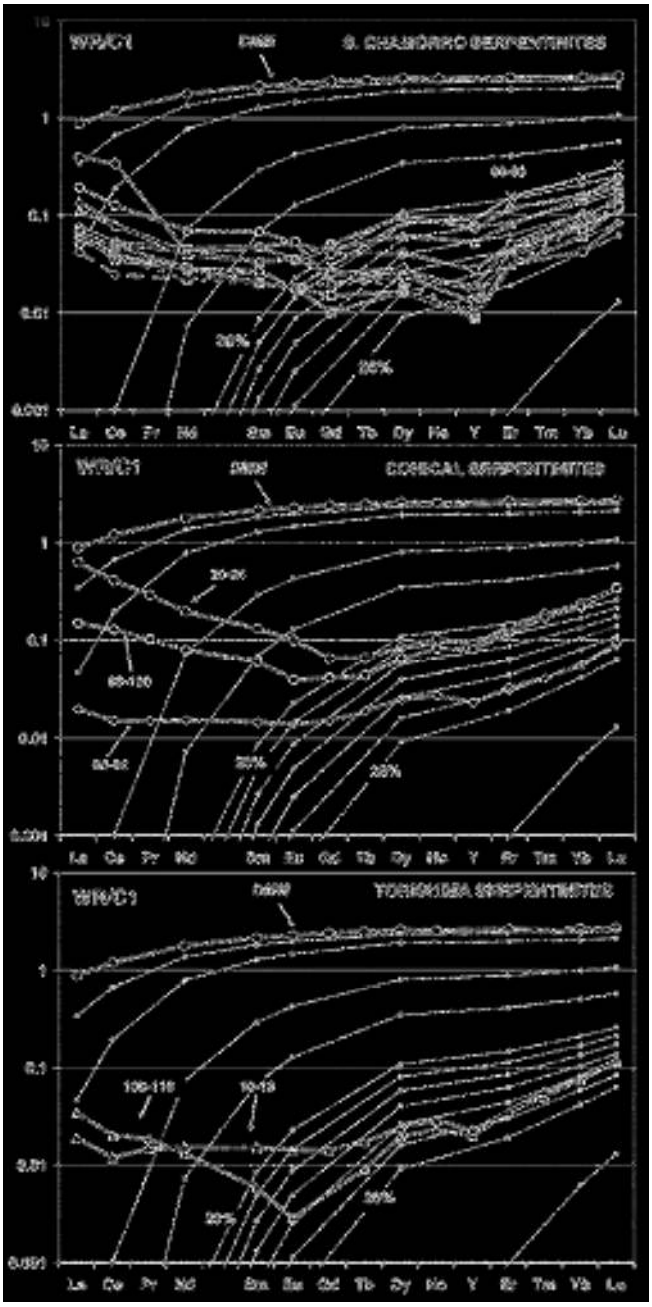

Fig. 5 - Chondrite-normalised REE abundance in peridotites from South Chamorro, Conical and Torishima Seamounts. C1-chondrite values are from Anders and Grevesse (1989). The chondrite-normalised REE abundance calculated for refractory peridotites after variable degrees of spinel-facies fractional melting of DMM are reported for comparison. Fractional melting equation was taken from Shaw (1970). Modal and geochemical composition of DMM were determined according to Hirschmann and Stolper (1996). Melting mode and solid/melt partition coefficients set were taken from Kinzler (1997; experiment at 1.5 GPa) and Ionov et al. (2002), respectively.

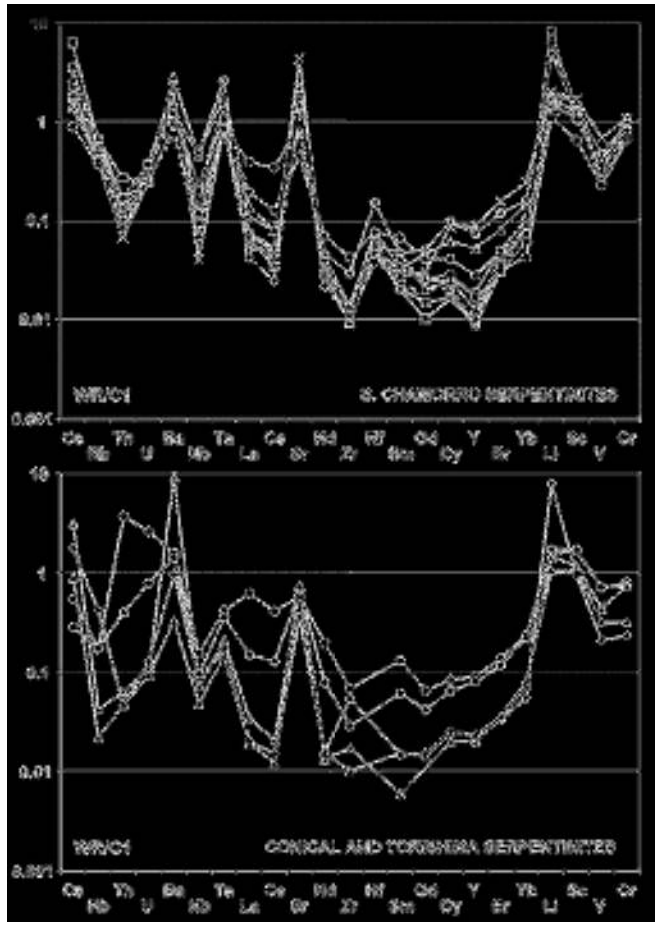

Fig. 6 - Chondrite-normalised incompatible trace elements diagrams for peridotites from South Chamorro, Conical and Torishima Seamounts. C1-chondrite values are from Anders and Grevesse (1989).

CaO content (21.8-22.3 wt%) has been found only in two grains from the harzburgite samples 195 1200A 17G1, 106-109 cm, and 195 1200A 6R1, 93-96 cm, which also show the lowest Mg# (0.927-0.930). Most orthopyroxenes are low to very low in CaO (< 1 down to 0.08 wt%), and significantly heterogeneous also within the same sample. Large CaO content is shown by the orthopyroxenes from 195 1200A 10R1, 90-93 cm harzburgite (1.5-2.6 wt.%). Although a general CaO decrease from the primary porphyroclasts to the secondary grains can be recognised, a significant CaO variability is, however, shown by the exsolved porphyroclasts on their own (Table 2). This variability is commonly observed in orthopyroxene from ophiolite peridotites (e.g., Rampone et al., 1995; Spadea et al., 2003).

The spinel composition straddles the spinel-chromite boundary with Cr# [expressed as Cr/(Cr + Al) molar] in the range of 0.37-0.66, and Fe^{3+}/Fe_T ratio from zero to 0.17. As a whole, the South Chamorro spinels are much more enriched in chromite component than those from abyssal peridotites (Fig. 7). Amphibole is magnesiohornblende to tremolite, consistently with the compositions previously documented by Parkinson and Pearce (1998) and Ohara and Ishii (1998).

The mantle minerals (Table 2) from Conical and Torishima Seamounts analysed in this study have the same major element characteristics as those from South Chamorro Seamount, and are also within or very close to the compositional fields defined by Parkinson and Pearce (1998). The olivine, orthopyroxene, and spinel from the Torishima Seamount peridotites show a rather homogeneous major element composition with Fo = 91.7, $Mg\#_{Opx}$ = 0.920-0.921, Al_2O_{3Opx} = 1.4-1.8 wt%, and $Cr\#_{Sp}$ = 0.53-0.56 (Figs. 7 and 8). The associated clinopyroxenes are characterised by appreciable Na_2O content (0.12-0.24 wt%). The minerals from the Conical Seamount peridotites are characterised by very large compositional variability (in particular of Al_2O_3). Consistently with the bulk-rock composition, the minerals from the pro-

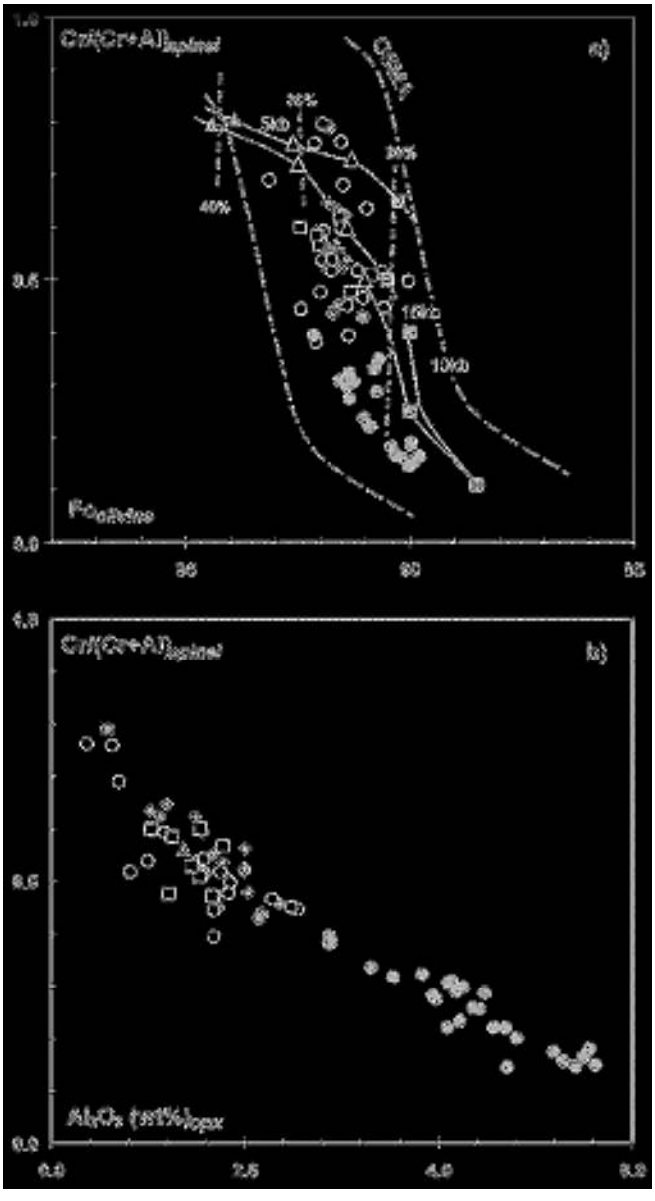

Fig. 7 - a) Fo index of olivine vs. Cr/(Cr+Al) of spinel for peridotites from Conical, Torishima and South Chamorro Seamounts. Symbols are as in figure 3. Moreover, the olivine-spinel mantle array (Arai, 1994) and the composition of peridotites investigated by Arai (1994) (lherzolite: empty squares; harzburgite: empty triangles; dunite: grey triangles), along with that of abyssal peridotites (Bryndzia and Wood, 1990; Johnson and Dick, 1992; Hellebrand et al., 2002: grey circles) are plotted for comparison. b) Al_2O_3 of orthopyroxene vs Cr/(Cr+Al) of spinel from the analysed peridotites. Grey circles are the composition of minerals from abyssal peridotites (Johnson and Dick, 1992; Hellebrand et al., 2002).

togranular 125 779A 22R1, 60-62 cm harzburgite have an overall more refractory composition (Fo = 91.8, $Mg\#_{Opx}$ = 0.922, Al_2O_{3Opx}~0.6 wt%, $Cr\#_{Sp}$ = 0.79) than the porphyroclastic harzburgites (Fo = 91.0-91.7, $Mg\#_{Opx}$ = 0.914, Al_2O_{3Opx} ~2.2 wt%, $Cr\#_{Sp}$ ~0.44). The very few clinopyroxenes found in the 125 779A 22R1, 60-62 cm harzburgite are characterised by a rather high Na_2O content (0.30-0.36 wt%).

DISCUSSION

The variability of the petrographic, mineralogical and geochemical features of bulk rock and mineral chemistry of the peridotites from the South Chamorro, Conical and Torishima Seamounts suggests that they underwent a complex, multistage evolution. As it will be stressed below, this evolution involved, at variable extent: partial melting, reactive porous flow melt migration, subsolidus metamorphic re-equilibration under decreasing T and open system conditions, and finally, serpentinisation. The latter is at present still affecting the peridotites (Mottl et al., 2003; Takano et al., 2004). Such a complex scenario requires a preliminary evaluation of the extension of chemical changes suffered by both bulk rocks and minerals as a consequence of mid to low T petrologic processes, in order to develop a critical sensibility on what the geochemical data can tell us about high T evolution of these mantle rocks.

Thus, in the following sections, it will be highlighted the role played by different processes in the definition of the present day geochemical composition of the peridotites object of this work.

Effects of the serpentinisation on the bulk rock composition

The large degrees of serpentinisation exhibited by the ultramafic samples of this study (Table 1) are similar to those previously reported by Ishii et al. (1992), Parkinson et al. (1992) and Parkinson and Pearce (1998) for Torishima and Conical Seamounts, and by Shipboard Scientific Party (2002) and D'Antonio and Kristensen (2004) for South Chamorro Seamount. The interstitial water recovered from South Chamorro, Conical and Torishima Seamounts has distinctive composition that implies an origin by dehydration of the subducting Pacific Plate (Mottl et al., 2003 and references therein). The temperature of the water emitted by springs on the seafloor is very low (~2°C in several IBM forearc seamounts; Mottl et al., 2003 and references therein), but an initial temperature of 150-250°C is argued for the fluids, when they are originated at the top of the subducting Pacific Plate, 27-29 km deep. On the basis of the lizardite + chrysotile + brucite paragenesis and the chemical characteristics of these minerals in South Chamorro Seamount peridotites, D'Antonio and Kristensen (2004) argued that serpentinisation must have occurred at temperatures not exceeding 200-300°C.

In our samples, as well as in those of Parkinson and Pearce (1998), the LOI index is positively correlated with MgO and negatively with SiO_2, CaO and Al_2O_3 (Fig. 4). These relationships evidence a clear dependence of LOI on the olivine modal content. Instead, no significant correlation is apparent with Na_2O and trace elements.

The effects of serpentinisation on major and trace element bulk rock composition are matter of debate. Some Ca mobilisation was calculated by Miyashiro et al. (1969) and Coleman (1971), whereas Snow and Dick (1995) showed that the abyssal serpentinites affected by low-T weathering can suffer Mg loss and Si enrichment. More recently, a nearly-isochemical character for the serpentinisation process has been stressed out in several papers (e.g., Scambelluri et al., 2001, Mevel, 2003, and references therein). As for Torishima and Conical samples, on the basis of the compositional variation of pore water with depth, Mottl et al. (2003) suggested that the underway serpentinisation takes up Si, Mg and Li, while Ca and Sr are removed by aragonite precipitation.

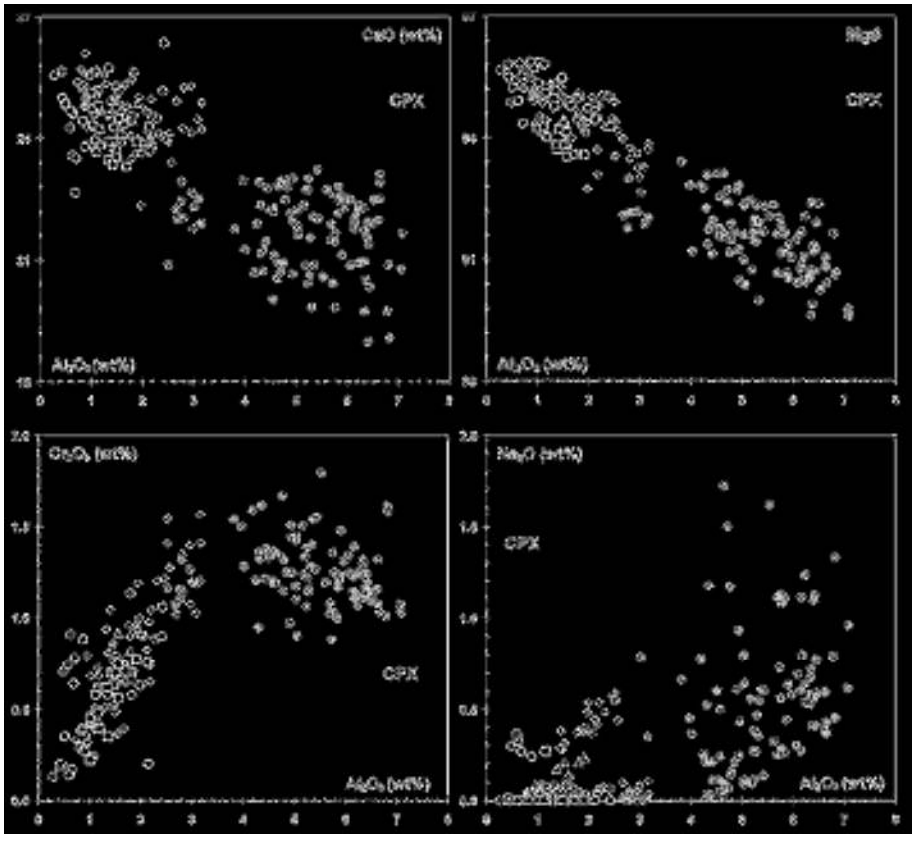

Fig. 8 - Al_2O_3 (wt%) vs. CaO (wt%), 100 x Mg#, Cr_2O_3 (wt%) and Na_2O (wt%) diagrams of clinopyroxene from Conical, Torishima and South Chamorro Seamounts. Symbols are as in Fig. 3. Grey circles are the composition of abyssal peridotites (Johnson et al., 1990; Johnson and Dick, 1992; Hellebrand et al., 2002; Seyler et al., 2001).

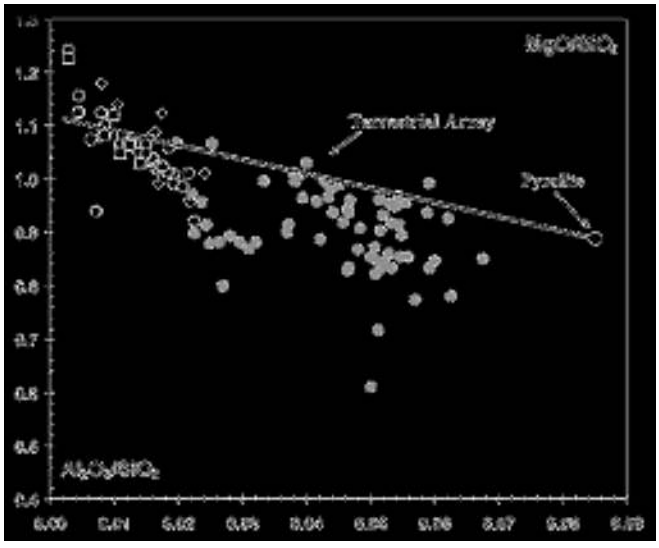

Fig. 9 - Al_2O_3/SiO_2 vs. MgO/SiO_2 diagram in peridotites from Conical, Torishima and South Chamorro Seamounts. The "terrestrial array" (Jagoutz et al., 1979; Hart and Zindler, 1986) are reported for discussion. Symbols are as in Fig. 3. Data for variably altered abyssal peridotites (grey circles) are from Snow and Dick (1995).

To verify the extension of the major element changes experienced by our samples during serpentinisation, they have been plotted, along with those reported by Parkinson and Pearce (1998), in the MgO/SiO_2 vs. Al_2O_3/SiO_2 diagram, in which fresh mantle peridotites define a linear trend (that is the "terrestrial array"; Jagoutz et al., 1979; Hart and Zindler, 1986). Fig. 9 shows that the Izu-Bonin-Mariana serpentinites straddle the "terrestrial array" suggesting that the ongoing serpentinisation produced, if it is the case, only limited changes in terms of SiO_2, MgO and Al_2O_3 content. This statement is also supported by the good to very good correlation occurring between the MgO and Al_2O_3 content of bulk rock and the major element mineral chemistry (in particular, with the $Cr\#_{Sp}$, the Al_2O_3 content of Opx and the olivine Fo). MgO content of bulk rock is also positively correlated with compatible trace elements (i.e. Co and Ni), but defines negative trends with moderately incompatible ones (i.e. Ga, Sc, V, Cr, HREE and Y). These compositional relationships are those commonly expected after melt-related processes. Instead, no significant correlation occurs between the MgO content and those of more incompatible trace elements such as L-MREE, LILE, HFSE and actinides. Parkinson et al. (1992) found that the IBM forearc peridotites containing most tremolite had also the highest La content. This evidence indicates that the moderately incompatible to compatible trace element composition of peridotites may reflect first-order high-temperature processes, whereas the concentration of highly incompatible elements must have been modified by relatively low-T processes.

Evidence for post-partial-melting mantle processes and their effects on mineral chemistry

The major element composition of the mantle pyroxenes from the peridotites of the South Chamorro, Torishima and Conical Seamounts is apparently more depleted in terms of Al, Na, Ti, Fe and richer in Ca, Si and Mg than those of abyssal peridotites far from trenches (Figs. 7 and 8). Consistently, olivine has high Fo content and spinel is particularly enriched in chromite component (namely in Cr and Fe^{2+}). The correlation among these different compositional parameters is good to very good, and is, in principle, consistent with very large degrees of partial melting (see experimental data and/or geochemical modelling in Jaques and Green, 1980; Hellebrand et al., 2001; Hellebrand and Snow, 2003).

On the other hand, most of the textural, mineralogical and chemical features shown by IBM forearc peridotites are clearly the result of post-melting evolution at lithosphere mantle conditions, involving both partial re-crystallisation during the percolation of exotic melts and subsolidus re-equilibration. In the following sections will be stressed out the possible role played by these processes in determining the peculiar mineral chemistry of the forearc peridotites.

The large effects of the subsolidus re-equilibration are unequivocally evidenced by the wealth of exsolution of orthopyroxene porphyroclasts and the anomalous low equilibrium T. Homogeneous T estimates are provided by the olivine-spinel Fe-Mg exchange thermometers (e.g. Fabries, 1979; Ballhaus et al., 1991; Table 3). The equilibrium T calculated according to the Ballhaus calibration are 670 ± 35°C, 699 ± 32°C and 700 ± 15°C for South Chamorro, Torishima and Conical peridotites, respectively. These data are similar to the T range estimated by Parkinson and Pearce (1998) using the same thermometer for Torishima (T = 646 ± 20°C) and Conical (T = 666 ± 19°C) peridotites, being 350-500°C lower than the T estimated for the abyssal peridotites (e.g. those reported by Brynzia and Wood, 1990). The witness of high-T mantle processes is still preserved in the random occurrence of Ca-rich areas in the core of porphyroclastic orthopyroxenes (T > 1200°C, according to the "Ca-in-Opx" thermometer of Brey and Kohler, 1990). Similar Ca-rich compositions are quite frequent in exsolved porphyroclastic orthopyroxenes from ophiolitic peridotites (e.g. Rampone et al., 1995; Spadea et al., 2003). The goodness of the orthopyroxene stoichiometry suggests that they are relic areas bearing compositional features inherited during high-T, early evolutionary stages rather than the result of random concentration of cryptic exsolution lamellae of clinopyroxene. In general, low equilibration temperatures point to low cooling rates (Zanetti et al., 1996, and references therein). Parkinson and Pearce (1998) argued that the low equilibration temperatures of Conical and Torishima peridotites are the result of diffusion subsolidus evolution in presence of water. Nevertheless, it will be shown below that the water content was very low during the South Chamorro mantle processes. Thus, it is alternatively proposed that the IBM forearc peridotites likely experienced slow a cooling rates due to a thermal flux exceeding that of normal Mid-Ocean-Ridges (MOR).

The post-melting interaction of the peridotites with interstitial melt at relatively high temperature is evidenced by: (1) the engulfed shape of porphyroclastic orthopyroxenes that are replaced by secondary mantle minerals; (2) the "magmatic" texture shown by the interstitial clinopyroxenes; (3) the (rare) occurrence of amphiboles in equilibrium with the secondary assemblage; (4) the relatively high Na concentration of the secondary clinopyroxene from some samples (e.g. from Torishima Seamount). The texture of the porphyroclastic orthopyroxenes from the Conical and Torishima peridotites has been first described and interpreted as the record of partial melting by Parkinson and Pearce (1998). The common presence of prismatic to round clinopyroxene in the embayed rims of orthopyroxene is a further evidence that such a texture has a reactive nature. This textural feature is ubiquitous in the abyssal peridotites (Hellebrand et al., 2002), as well as in ophiolitic massif (Piccardo et al., 2006), and provides evidence for the peridotite reaction with percolating melt (Suhr and Edwards, 2000).

Straightforwardly referred to the low equilibrium temperatures can be the very large Ca content of clinopyroxene (Fig. 8a). Subsolidus equilibration at low T can also explain

Table 3. Estimates of equilibrium temperature and oxygen fugacity.

LEG	Hole	Core	Interval	*Fo (Ol)*	*Cr# (Sp)*	Al_2O_3(wt%) *(Opx)*	T (°C) *(1)*	T (°C) *(2)*	*fO2* (ΔlogFMQ) *(3)*	*fO2* (ΔlogFMQ) *(4)*
SOUTH CHAMORRO										
195	1200A	3R1	49-52	0.916	0.634	1.03	689	639	-2.32	-1.48
195	1200A	3R1	88-91	0.914	0.623	1.49	708	661	-0.44	0.25
195	1200A	6R1	93-96	0.918	0.519	2.00	696	653	-1.88	-1.04
195	1200A	6R2	66-69	0.915	0.524	2.00	756	723	-1.59	-1.00
195	1200A	7R2	61-67	0.919	0.562	2.00	774	738	-0.45	0.31
195	1200A	10R1	42-45	0.921	0.593	1.57	720	676	-0.61	0.20
195	1200A	10R1	90-93	0.915	0.457	2.36	716	678	-1.96	-1.12
195	1200A	13R1	41-44	0.913	0.478	2.04	712	671	-0.93	-0.22
195	1200A	14R1	22-24	0.916	0.430	1.73	676	635	-0.22	0.51
195	1200A	16R2	12-15	0.916	0.552	1.68	697	654	-1.50	-0.70
195	1200A	17G1	106-109	0.915	0.535	1.77	729	684	-0.41	0.36
195	1200B	1W1	56-59	0.918	0.647	1.17	720	673	-0.34	0.53
195	1200A	13R1	59-61	0.915	0.623	1.13	666	615	-0.53	0.30
CONICAL										
125	779A	22R1	60-62	0.918	0.790	0.59	795	758	-0.25	0.66
125	779A	26R2	20-24	0.916	0.437	2.18	730	693	-0.20	0.78
125	779A	26R2	98-100	0.910	0.429	2.15	720	683	-0.69	0.07
TORISHIMA										
125	784A	45RCC	10-13	0.917	0.526	1.76	751	709	0.76	1.43
125	784A	45R1	108-110	0.917	0.562	1.37	733	689	0.35	1.00

Temperatures shown have been calculated on the basis of the Fe-Mg exchange thermometers of (1) Fabriès et al. (1979) and (2) Ballhaus et al. (1991). Oxygen fugacity has been calculated on the basis of the calibration of (3) Ballhaus et al. (1991) and (4) Brindzia and Wood (1990) at an arbitrary pressure of 1 GPa and using the temperature from the thermometer of Ballhaus.

the very large Mg# of clinopyroxene (that is matched by secondary orthopyroxene and olivine: see also Parkinson and Pearce, 1998). Nevertheless, a similar results can be potentially obtained by interaction with refractory melts (Bodinier and Godard, 2003), such as the regionally-relevant boninites.

Another compositional feature worth of mentioning shown by the mineral chemistry of IBM forearc peridotites is the low to extremely low Al and Cr content of pyroxenes. In general, it reflects the overall depletion of these two elements in the bulk rock, whose meaning will be addressed in the paragraph 7.4. The Cr# of spinel is strictly correlated with that of the associated of both clinopyroxene and orthopyroxene, thus evidencing the active buffering role exerted by the oxide. A concomitant decrease of Al and Cr content, as shown by the pyroxenes from the IBM forearc peridotites, is expected for extremely large degrees of partial melting (Hellebrand and Snow, 2003). However, the heterogeneity of the Al and Cr contents within the same sample, which reach the minimum concentration level in interstitial grains in equilibrium with chromite, must be related to subsolidus re-equilibration and/or melt-peridotite interaction at relatively shallow conditions (e.g. Zanetti et al., 1996; Seyler et al., 2001). Again, it can be guessed that such a decrease can be stronger in presence of refractory melts. As a whole, it is concluded that the peculiar refractory character of the mineral chemistry of IBM forearc peridotites was further accentuated by the exceptional intensity of post-melting processes, which included reaction with melts and very low equilibration T.

Estimates of the degree of partial melting

Parkinson and Pearce (1998) interpreted the Conical harzburgites as residual MORB mantle after 15-20% fractional melting, which has subsequently been modified by interaction with boninitic melt within the mantle wedge. Conversely, Torishima peridotites were considered the result of 20-25% fractional melting in a supra-subduction zone environment.

The HREE composition of the South Chamorro peridotites is consistent with 20-26% fractional melting of Depleted MORB Mantle (DMM; Fig. 5), whereas 20 to 30-33% of partial melting can be estimated according to the MgO content and extrapolating the modelling curves of Niu (1997) at higher MgO value. Again, 25-28% partial melting can be calculated on the basis of the Fo and $Cr\#_{Sp}$ according to Arai (1994). Similar degrees of partial melting (20-25%) were estimated by Shipboard Scientific Party (2002) on the basis of CaO and Al_2O_3 contents, and Mg# of Site 1200 bulk rocks analysed onboard during ODP Leg 195.

As for the Torishima harzburgites here studied, the HREE fractionation and content (in the range Dy-Lu) of the whole rock agree strictly with those modelled for refractory residua after 24-25% fractional melting of spinel facies DMM. This degree of basalt removal is very similar to that estimated on the basis of: i) the Fo content (24-27%) according to Arai (1994); ii) the modal Cpx content (~25% partial melting: e.g. Niu, 1997); iii) the MgO content of the bulk rock (20-23% partial melting) according to Niu's calculation. Conversely, slightly lower degrees of partial melting (18%) are obtained using the empirical equation of Hellebrand et al. (2001) based on the Cr# of spinel.

Bulk rock MgO and HREE content compositions, as well as the Fo content, indicate that sample 125 779A 22R1, 60-62 cm from Conical Seamount has suffered ~25% fractional melting under spinel facies conditions. Similar large partial melting degrees (22%) are calculated on the basis of the $Cr\#_{Sp}$. More fertile composition are displayed by samples 125 779A 22R2, 98-100 cm and 125 779A 22R2, 20-24 cm. On the basis of the MgO composition and the different trend of partial melting calculated by Niu, the estimated degree of partial melting under spinel facies is 14-15% and 17-18% for 125 779A 22R2, 98-100 cm and 125 779A 22R2, 20-24 cm, respectively. In the 125 779A 22R2, 20-24 cm harzburgite, the decrease of MgO composition is accompanied by a slight increase of Fo and a decrease of orthopyroxene contents, although with an increase of clinopyroxene (around 4% by vol.). This observation cannot be accounted for by a larger degree of partial melting, likely indicating more intense melt-peridotite interaction. In these two samples, the HREE content is more steeply fractionated with respect to that expected for the pertinent concentration level in residua after spinel facies fractional melting. In particular, the HREE content crosscut the HREE composition of modelled refractory peridotites after 19-24% partial melting of spinel-facies DMM.

High-T mantle evolution

Fig. 3a shows that all the peridotites collected from the Torishima, Conical and South Chamorro Seamounts form a homogeneous array spanning from a compositional field pertinent to high degrees of isobaric batch and/or polybaric fractional melting to a region extremely MgO-enriched and SiO_2-depleted. Such an array is significantly different with respect to the whole trend shown by the abyssal peridotites far from trenches (see data and references reported by Niu, 1997; Asimow, 1999; Baker and Beckett, 1999), thus likely representing a distinctive compositional feature. This distribution indicates that the IBM forearc peridotites experienced an early stage of strong depletion under the petrologic parameters (i.e. T, P, melting mode etc.) expected to govern the adiabatic upraise of an asthenospheric sector, followed by a second stage of depletion characterised by a more pronounced impoverishment in pyroxenes (in particular, orthopyroxene).

An overall depletion in SiO_2 for a given MgO content, with respect to that calculated for refractory residua after partial melting is typical of the abyssal peridotites. This feature has been interpreted as the product of interaction between migrating melts and residual peridotites, either by equilibrium porous flow, refertilisation or olivine crystallisation at relatively shallow level (e.g. Kelemen et al., 1997; Niu, 1997; Asimow, 1999). Similarly, the array defined by IBM forearc peridotites might indicate that in the second stage of depletion their chemical and modal composition was variably, but sometimes significantly, modified by porous flow melt percolation at relatively shallow levels that impoverished them in pyroxenes.

On the other hand, several petrochemical features of the IBM peridotites forearc cannot straightforwardly accounted for by late interaction with upraising MORB. In particular, bulk rock MgO content is positively and negatively correlated with the olivine Fo content and the Al_2O_3 content of bulk rock, respectively. The Al_2O_3 content of the peridotite minerals (i.e. spinel and pyroxenes) varies consistently with that of bulk rock (Fig. 10a, b), being the latter also positively correlated with the bulk rock concentration of the moderately incompatible trace elements, such as Cr, V, Sc, Y and HREE (Fig. 10c). Besides, the Al_2O_3 composition of bulk

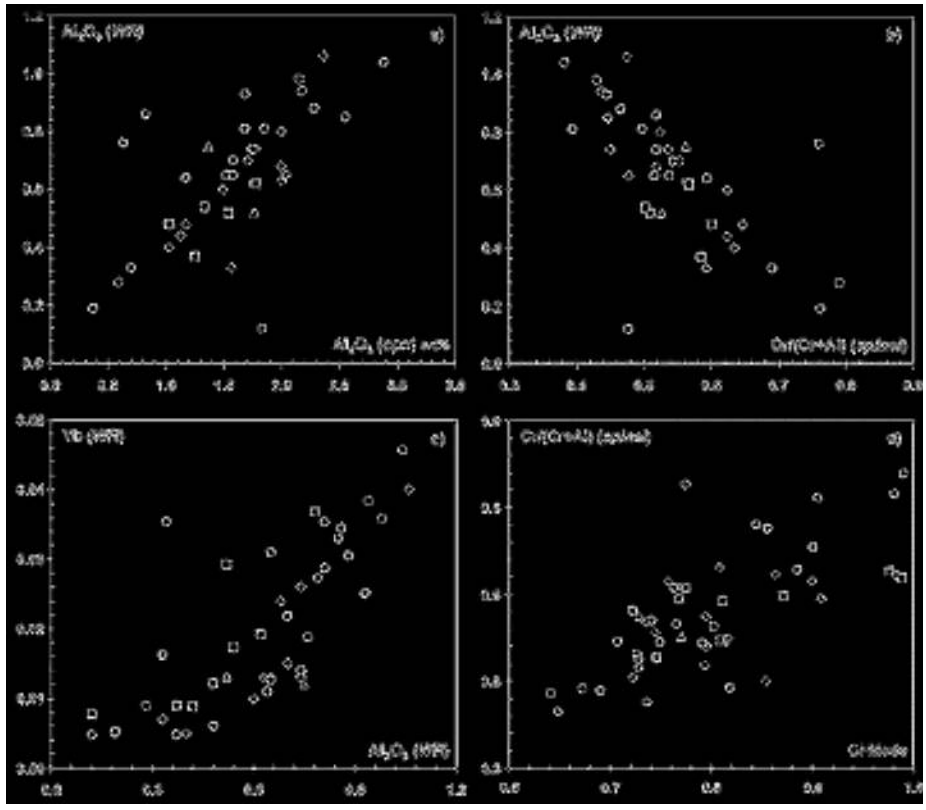

Fig. 10 - Covariance of the petrochemical features of the IBM forearc peridotites. a) Al_2O_3 content of whole rock vs. Al_2O_3 content of orthopyroxene (wt%); b) Al_2O_3 content of whole rock (wt%) vs. molar Cr/Cr+Al) of spinel; c) Al_2O_3 (wt%) vs. Yb (ppm) content of whole rock; d) Olivine modal content (by Vol.%) vs. molar Cr/Cr + Al) of spinel. Symbols as in Fig. 3.

rock and minerals is negatively correlated with the estimated olivine modal content (Fig. 10d) and positively correlated with the modal composition of both pyroxenes.

Such compositional relationships are those typically expected in refractory residua after different degrees of partial melting (e.g. Mysen and Kushiro, 1977; Jaques and Green, 1980; Hirose and Kawamoto, 1995; Ozawa and Shimizu, 1995; Niu, 1997). In contrast, they are lacking in peridotites deeply re-equilibrated as a consequence of the upraising MORB, where the composition of the minerals is relatively enriched in Al_2O_3 and points to approach the chemical equilibrium with the percolating melts (Rampone et al., 2004; Piccardo et al., 2004a; 2004b; 2005; 2006).

How can these different lines of evidence be reconciled?

In principle, it can be taken into account that two petrologic features believed to characterise the partial melting of mantle peridotites in SSZ environment might play a role in determining the relative SiO_2 depletion documented in the IBM forearc peridotites. The first feature is the thermal conditions of partial melting argued for the forearc peridotites. There is now a general consensus about the fact that their melting has to occur under thermal conditions higher than those of Mid-Ocean-Ridges far from mantle plumes (Flower et al., 2001; Niu et al., 2003). The second issue concerns the common wisdom that the melting of the forearc peridotites takes place under hydrous conditions, owing to the addition of hydrous fluids/melts containing slab-derived components (Bonatti and Michael, 1989; Ozawa and Shimizu, 1995; Grove et al., 2003). Both petrologic features can potentially perturb the melting mode and consequently the major element compositional trends. As for the effects of exceptionally large T conditions, since the petrologic investigation by Mysen and Kushiro (1977), it is expected that, under anhydrous melting conditions, the exhaustion of clinopyroxene is followed by a significant increase of the orthopyroxene contribution to the melting process, which should lead to its exhaustion after a relatively small interval of partial melting.

The effects on melting mode induced by the addition of water during a melting process are much more articulated. It is well known that it increases significantly the melt productivity, in particular at high temperature (Hirose and Kawamoto, 1995; Gaetani and Grove, 1998; Hirschmann et al., 1999), as a consequence of the slope decrease of solidus boundary (see Mysen and Kushiro, 1977). Pertinent to the apparent array of the IBM peridotites is that the water-bearing partial melting determines the incongruent melting of orthopyroxene, at least up to 3 GPa (Kushiro, 1990), thus likely determining an apparent excess of olivine in the refractory residue with respect to anhydrous conditions.

The effects of both high-T and hydrous condition on the modal variation of the refractory residua are expected to be still stronger during partial melting at low P, as a consequence of the expansion of the stability field of olivine (e.g. Niu, 1997; Gudfinnsson and Presnall, 2000; Grove et al., 2003). Very low mean melting pressure values (P_M) have been calculated by Niu (1997) for the abyssal peridotites close to hotspot (P_M ~0.5 GPa). Very low melting pressure for IBM peridotites may be consistent with the significant Al_2O_3 depletion exhibited by both bulk rock and mineral composition even by the more fertile peridotites (Figs. 3b and 7). Nevertheless, the partial melting of a clinopyroxene-free spinel harzburgite requires $T \geq 1400°C$ at 1 GPa (e.g. Hirschmann et al., 1999), which are very different with respect to those argued for segment-ends of MOR and plumes (White, 1988). Thus, this hypothesis is so far not sufficiently constrained by the petrologic models.

According to Parkinson and Arculus (1999), very low water contents (0.030-0.075 wt% H_2O) are sufficient to produce a valuable increase of the oxidation state. Thus, it is expected that the occurrence of hydrous melting is denounced by an increase of the oxygen fugacity in the residual peridotites. The oxidised conditions of the Torishima peridotites are consistent with such a scenario (Fig. 11). Conversely, the estimates of the oxygen fugacity of South

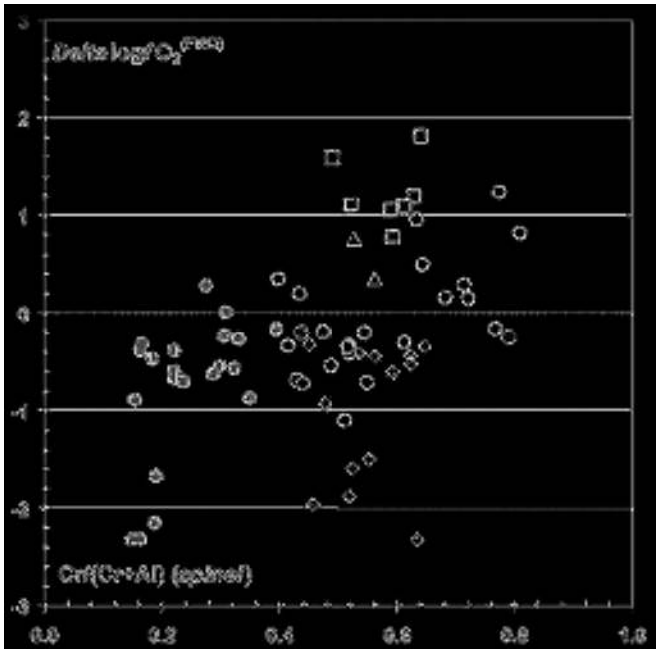

Fig. 11 -. Plot of $\Delta \log fO_2^{(FMQ)}$ vs. Cr/(Cr + Al) of spinel for peridotites from Conical, Torishima and South Chamorro Seamounts (Parkinson and Pearce, 1998; This study). As for the samples of This Study, it is plotted the estimate of the oxygen fugacity according to the calibration of Ballhaus et al. (1991). Symbols are as in Fig. 3. The fugacity conditions estimated for abyssal peridotites (grey circles: Bryndzia and Wood, 1990; Johnson and Dick, 1992; Hellebrand et al., 2002) are plotted for comparison.

Chamorro peridotites and Conical harzburgites fall in the fO_2 field related to the abyssal peridotites (geothermometer by Ballhaus et al., 1991) (Fig. 11) or point to only slightly more oxidised conditions, according to the calibration of Bryndzia and Wood (1990). The differences of the redox equilibrium conditions between Conical and Torishima were already highlighted by Parkinson and Pearce (1998), who also found that the dunites from both Seamounts are meanly more oxidised than harzburgites, with the Conical dunites defining a range similar to that of Torishima harzburgites. This correlation between modal composition and oxygen fugacity conditions is not present in the South Chamorro samples (Fig. 11). Based on the differences in terms of oxygen fugacity, Parkinson and Pearce (1998) proposed that the entire Torishima mantle experienced partial melting in presence of slab-derived components in supra-subduction setting, whereas the Conical mantle wedge escaped this event, thus maintaining a pristine "abyssal peridotite" signature. As a consequence, the relatively reduced conditions shown by South Chamorro peridotites seem to exclude that hydrous partial melting is responsible for the array in the SiO_2-MgO diagram shown by the IBM forearc peridotites.

Thus, to reconcile all the petrochemical data it is proposed that the strong impoverishment in orthopyroxene was accomplished during the reactive upraise of melts extremely depleted in fusible elements, such as Al, Ti and REE, through less refractory mantle columns. The possible relevance of late melt-peridotite interactions in the evolution of IBM forearc peridotites was previously pointed out by Parkinson and Pearce (1998), who related the petrogenesis of dunites recovered from the Conical Seamount to a late percolation of boninite melt through an original MORB mantle column. A similar scenario has been successively proposed to explain the origin of the dunite bodies in other world-wide SSZ ophiolite sequences (as for the Indus Suture Zone, see Sachan, 2001; Zhou et al., 2005). In particular, the progressive evolution of the composition of the extracted and/or migrating melts from MORB to ultra-depleted (postulated to have boninitic affinity) is spectacularly documented in sections of the Bay of Islands ophiolite (Newfoundland, Canada; Suhr et al., 1998; Suhr, 1999; Suhr and Edwards, 2000; Suhr et al., 2003).

Independently on the nature of the ultra-depleted melts, which is matter of debate (primary melts in equilibrium with harzburgitic residua or transient composition produced by melt-peridotite interactions?; see Vernières et al., 1997), the compositional evolution towards SiO_2-depleted and MgO-enriched compositions and the petrographic features indicate that they moved through reactive porous flow at relatively low P (Niu, 1997).

Thus, to account for the complex combination of petrochemical evidence shown by IBM forearc peridotites, a general, three-stages-model is proposed for their high-T evolution. It involves:

1) an early depletion event, during which the IBM forearc peridotites experienced 20-25% polybaric fractional melting during adiabatic upwelling;

2) a second depletion event characterised by a marked impoverishment in modal orthopyroxene, triggered by the upraise migration of ultra-depleted melts;

3) a late interaction between relatively small volume of migrating melt and the refractory mantle sequence.

This model is similar to that envisaged by Suhr and Edwards (2000) for documenting the evolution of the arc-related section of the Bay of Islands ophiolite (Newfoundland, Canada), in which the second stage is argued to be characterised by open-system partial melting rather than reactive porous flow. The evidence of a multistage evolution led Parkinson and Pearce (1998) to exclude that Conical peridotites could be the source of arc magmatism. Consistently, Niu et al. (2003) exclude the possibility that the mantle source of arc magmatism can be rapidly brought to the surface by tectonics in a forearc area linked to roll-back subduction.

The acknowledge of the first stage is based on the observation that the less-refractory IBM forearc peridotites lie on the trends describing the decompression melting of uprising fertile (asthenospheric) mantle. During this stage, IBM forearc peridotites were actual mantle sources. The average degrees of depletion is higher than that observed in abyssal peridotites, thus indicating particularly hot geotherms. Figs. 3a and c show that at the end of this process the peridotites preserved SiO_2/MgO ratios consistent with the melting trends argued for abyssal peridotites at MOR, but acquired the typical, very strong, Al_2O_3 depletion, which is a characteristic feature of the forearc peridotites. This evidence may be explained by very low closure P of the melting process and suggests a close genetic linking to the onset of arc magmatism. The second stage occurred at relatively lower pressures, when the IBM peridotites were likely emplaced above the actual source region of the extracted melts. This stage is guessed to be firmly related to arc volcanism. Nevertheless, the progressive change of the oxidation state of the mantle minerals, that meanly decreases from the Torishima Seamount (northern Izu-Bonin forearc) to the South Chamorro (southern Mariana forearc), through the Conical Seamount (northern Mariana forearc), highlights the presence of a marked gradient in terms of contributions coming from the subducted Pacific Plate during this phase. Consistently, it is argued that the melts composition was boninitic

at Torishima to become apparently ultra-depleted MORB at South Chamorro.

The third stage is that more easily recognisable. It determined the petrographic and mineralogical features ubiquitously present in the IBM forearc peridotites (e.g. crystallisation of late clinopyroxene, embayment of the orthopyroxene porphyroclasts), and likely marks the accretion of the mantle sequence to the thermal boundary layer. It was accompanied by the development of transient geochemical gradients in the migrating liquids (at present recorded by clinopyroxene compositions) as a consequence of chromatographic-type chemical exchange with the peridotite (Suhr and Edwards, 2000; Zanetti et al., in prep).

Geodynamic implications

The most recent hypotheses on the genesis of the SSZ magmatism (and, in particular, of the boninites) and of the geological conditions allowing for the onset of intra-oceanic subduction involve the occurrence of a positive thermal anomaly in the mantle determined by asthenosphere upwelling. For instance, a relevant role for plume activity has been proposed to be related to the boninite magmatism in the IBM area (e.g. Macpherson and Hall, 2001). Kohut et al. (2006) guess that the asthenospheric wedge is not only hydrated by the fluids from the downgoing slab, but also experiences significant upwelling, as typical of rift zones or hotspots. In a different perspective, the "plume activity" has been invoked by Niu et al. (2003), who attribute the initiation of intra-oceanic subduction to the collision of an unsubductable oceanic plateau, consisting of the refractory residuum left by extremely large degrees of partial melting localised in the "head" of uprising plumes and the associated, thick, basaltic crust. Recently, a role for an Ocean Island Basalt-type (i.e., plume) mantle in the genesis of both West Philippine Basin basalts and arc volcanics of the Palau-Kyushu Ridge (ODP Site 1201; Fig. 1) has been ruled out on geochemical and isotopic grounds (Savov et al., 2006); however, there is no doubt about the occurrence of an important thermal anomaly during the early stages of magmatism at IBM.

A fundamental role of the asthenosphere flow in the generation of depleted forearc peridotites and boninites has been also pointed out by Flower et al. (2001), Flower and Dilek (2003) and Dilek and Flower (2003), although in the frame of a more comprehensive model. In particular, they consider that subduction nucleation and arc-trench rollback cycles are triggered by the effects of subhorizontal mantle flow resulting either directly from the collision-induced asthenosphere extrusion, or indirectly via collision-induced plate cinematic adjustments. The mantle extrusion is specifically supported by geologic and petrologic evidence from IBM forearc, which may be viewed as lithologic and geochemical 'high-tide mark' delimiting distal mantle extrusion effects, and by the spatial-temporal variation of isotopic mantle contaminants beneath the eastern Eurasia-western Pacific region (Flower et al., 2001).

Our data confirm that the entire evolution of the IBM forearc peridotites was characterised by a pronounced positive thermal anomaly. Besides, the oxidised conditions of Torishima harzburgites suggest that the overall depletion referred to Stage 1 was already related to the arc formation. The reduced state argued for the ultra-depleted melts characterising the Stage 2 of the South Chamorro mantle column provides the evidence that the addition of slab-derived components was not the "engine" of the process. Thus, the positive thermal anomaly had to persist throughout the main stages of depletion and was strictly related to the arc formation. In this frame, it is proposed that IBM peridotites during Stage 1 underwent decompression partial melting and contributed to arc volcanism as actual mantle source. Successively, they were emplaced at relatively shallow levels (Stage 2), constituting the top of a strongly refractory mantle column and being percolated by melts produced by plumbing sources of the arc volcanism.

CONCLUDING REMARKS

The petrographic and geochemical characterisation of mantle peridotite fragments recovered at the top of the South Chamorro Seamount (located in the southernmost part of the Mariana forearc) and the comparison of their petrochemical features with those of analogue samples from Conical Seamount and Torishima Seamount (located in the northern sector of the Mariana forearc and in the Izu-Bonin forearc, respectively) allow us to propose the following, comprehensive, scenario for the petrochemical evolution of the IBM forearc peridotites.

(1) The mantle peridotites from Izu-Bonin and Mariana forearc have experienced a similar first evolution stage characterised by 20-25% partial melting. At the end of this process the peridotites had SiO_2/MgO ratios consistent with the melting trends argued for abyssal peridotites at MOR, but acquired the typical, very strong, Al_2O_3 depletion, which is a characteristic feature of the forearc peridotites. This evidence may be explained by very low closure P of the melting process and suggests a close genetic linking to the onset of arc magmatism. Residual harzburgites from South Chamorro and Conical Seamounts in the Mariana forearc recording this evolution stage show reduced conditions, similarly to abyssal peridotites. This observation suggests that the large partial melting was not triggered by the upwelling of slab-derived components. Alternatively, it was presumably related to the adiabatic upwelling of a hot asthenosphere up to very shallow depths.

(2) A second evolution stage (Stage 2) was characterised by a further increase of the refractory character of the peridotites, at which is associated a consistent compositional changes of the mineral chemistry. Nevertheless, this stage produced harzburgites and orthopyroxene-bearing dunites with SiO_2/MgO ratios significantly lower than that argued for partial melting of an ascending adiabatic mantle. To reconcile all the petrochemical evidence, it is proposed that this evolution stage was related to the migration of ultra-depleted melts coming from deeper sources. The oxidised state of the SiO_2-depleted peridotites from Conical and Torishima Seamounts suggests that they were percolated by melts containing slab-derived components. It is also likely that the percolation of oxidised melts could have determined the overall oxidation of the mantle column beneath the Torishima Seamount. Conversely, the reduced conditions of the SiO_2-depleted peridotites from South Chamorro Seamounts points to a virtual absence of crustal components in the late ultra-refractory melts. This represents a further evidence that also the Stage 2 was characterised by a regional thermal excess rather than to be related to the injection of slab-derived liquids.

(3) The olivine + orthopyroxene + spinel porphyroclastic mineral assemblages developed during the Stages 1 and 2. The crystallisation of the clinopyroxene-bearing ones is ap-

parently related to late events of melt migration (Stage 3), possibly related to Stage 2. It is proposed that the very large subsolidus re-equilibration recorded by the IBM forearc peridotites is the evidence of a very slow cooling rate due to the persistence of a large thermal flux rather than an effect of fluid activity, as previously argued by Parkinson and Pearce (1998). If it is the case, this would be a further indication consistent with the existence of a positive thermal anomaly during the entire mantle evolution of the IBM forearc peridotites. Both the interaction of the peridotites with ultra-refractory melts and the large subsolidus re-equilibration at low P were functional to increase the Al-depleted character of the spinel and pyroxenes.

(4) As a whole, the petrochemical features exhibited by the IBM forearc peridotites suggest that the establishment and development of the arc magmatism was related to the occurrence of a positive thermal anomaly that expanded the main stage of partial melting of the ascending asthenosphere (Stage 1) at very shallow levels. The addition of slab-derived components is apparent only locally and in a second stage (Stage 2). Consistently, it is proposed that a regional upraise of the asthenosphere along the western margin of the Pacific Ocean was the main geodynamic feature responsible for the onset of the intra-oceanic subduction.

ACKNOWLEDGEMENTS

This paper benefited of the revisions carried out by Massimo Coltorti and Yildrem Dilek, who are greatly thanked.

REFERENCES

Anders F. and Grevesse N., 1989. Solar system abundances of the elements: meteoritic and solar. Geochim. Cosmochim. Acta, 53: 197-214.

Arai S., 1994. Characterization of spinel peridotites by olivine-spinel compositional relationships: review and interpretation. Chem. Geol., 113: 191-204.

Asimow P.D., 1999. A model that reconciles major- and trace-element data from abyssal peridotites. Earth Planet. Sci. Lett., 169: 303-319.

Baker M.B. and Beckett J.R., 1999. The origin of abyssal peridotites: a reinterpretation of constraints based on primary bulk compositions. Earth Planet. Sci. Lett., 171: 49-61.

Ballhaus C., Berry R.F. and Green D.H., 1991. High pressure experimental calibration of the olivine-orthopyroxene-spinel oxygen geobarometer: implications for the oxidation state of the upper mantle. Contrib. Mineral. Petrol., 107: 27-40. (Erratum 1: Ballhaus C., Berry R.F. and Green D.H., 1991. Contrib. Mineral. Petrol., 108: 384; Erratum 2: Ballhaus C., Berry R.F. and Green D.H., 1994. Contrib. Mineral. Petrol., 118: 109).

Bonatti E. and Michael P.J., 1989. Mantle peridotites from continental rifts to ocean basins to subduction zones. Earth Planet. Sci. Lett., 91: 297-311.

Brey G.P. and Köhler T., 1990. Geothermobarometry in four-phase lherzolites II. New thermobarometers, and practical assessment of existing thermobarometers. J. Petrol., 31 (6): 1353-1378.

Bryndzia L.T. and Wood B.J., 1990. Oxygen thermobarometry of abyssal peridotites: The redox state and C-O-H volatile composition of the Earth's sub-oceanic upper mantle. Am. J. Sci., 290: 1093-1116.

Bodinier J.-L. and Godard M., 2003. Orogenic, ophiolitic, and abyssal peridotites. Treatise on geochemistry: Vol. 2. The mantle and the core, p. 103-170.

Coleman R.G., 1971. Plate tectonic emplacement of upper mantle peridotites along continental edges. J. Geophys. Res., 76: 1212-1222.

D'Antonio M. and Kristensen M.B., 2004. Serpentine and brucite of ultramafic clasts from the South Chamorro Seamount (Ocean Drilling Program Leg 195, Site 1200): inferences for the serpentinization of the Mariana forearc mantle. Mineral. Mag., 68 (6): 887-904.

Dilek Y. and Flower M.F.J., 2003. Arc-trench rollback and forearc accretion: 2. A model template for ophiolites in Albania, Cyprus, and Oman. In: Y. Dilek and P.T. Robinson (Eds.), Ophiolites in Earth history. Geol. Soc. London Spec. Publ., 218: 43-68.

Deschamps A. and Lallemand S., 2002. The West Philippine Basin: an Eocene to Early Oligocene back-arc basin opened between two opposed subduction zones. J. Geophys. Res., 107: 2322-2346.

Fabriès J., 1979. Spinel-olivine geothermometry in peridotites from ultramafic complexes. Contrib. Mineral. Petrol., 69 (4): 329-336.

Flower M.F.J., Russo R.M., Tamaki K. and Hoang N., 2001. Mantle contamination and the Izu-Bonin-Mariana (IBM) "high-tide mark": evidence for mantle extrusion caused by Tethyan closure. Tectonophysics, 333: 9-34.

Flower M.F.J. and Dilek Y., 2003. Arc-trench rollback and forearc accretion: 1. A collision-induced mantle fow model for Tethyan ophiolites. In: Y. Dilek and P.T Robinson. (Eds.), Ophiolites in Earth History. Geol. Soc. London Spec. Publ., 218: 21-41.

Fryer P. and Pearce J.A., 1992. Introduction to the scientific results of Leg 125. In: P. Fryer, J.A. Pearce, L.B. Stokking et al. (Eds.). Proceed. O.D.P. Sci. Res., 125: 3-11.

Fryer P., 1992a. Mud volcanoes of the Marianas. Sci. Am., 266: 46-52.

Fryer P., 1992b. A synthesis of Leg 125 drilling of serpentine seamounts on the Mariana and Izu-Bonin forearcs. In: P. Fryer, J.A. Pearce, L.B. Stokking et al. (Eds.), Proc. O.D.P. Sci. Res., 125 (1): 593-614.

Fryer P., 1996. Evolution of the Mariana convergent plate margin system. Rev. Geophys., 34: 89-125.

Fryer P., Wheat C.G. and Mottl M.J., 1999. Mariana blueschist mud volcanism: implications for conditions within the subduction zone. Geology, 27: 103-106.

Fujioka K., Okino K., Kanamatsu T., Ohara Y., Ishizuka O., Haraguchi S. and Ishii T., 1999. Enigmatic extinct spreading center in the West Philippine backarc basin unveiled. Geology, 27: 1135-1138.

Gaetani G.A. and Grove T.L., 1998. The influence of water on melting of mantle peridotite. Contrib. Mineral. Petrol., 131: 323-346.

Grove T.L., Elkins-Tanton L.T., Parman S.W., Chatterjee N., Muentener O. and Gaetani G.A., 2003. Fractional crystallisation and mantle-melting controls on calc-alkaline differentiation trends. Contrib. Mineral. Petrol., 145: 515-533.

Gudfinnsson G.H. and Presnall D.C., 2000. Melting behaviour of model lherzolite in the system CaO-MgO-Al_2O_3-FeO at 0.7-2.8 GPa. J. Petrol., 41 (8): 1241-1269.

Hall R., Ali J.R., Anderson C.D. and Baker S.J., 1995. Origin and motion history of the Philippine Sea Plate, Tectonophysics, 251: 229-250.

Hall R., 2002. Cenozoic geological and plate tectonic evolution of SE Asia and the SW Pacific: computer-based reconstructions, model and animations. J. As. Earth Sci., 20: 353-431.

Hart S.R. and Zindler A., 1986. In search of a bulk Earth composition. Chem. Geol., 57: 247-267.

Hellebrand E., Snow J.E., Dick H.J.B. and Hofmann A.W., 2001. Coupled major and trace elements as indicators of the extent of melting in mid-ocean-ridge peridotites. Nature, 410: 677-680.

Hellebrand E., Snow J.E., Hoppe P. and Hofmann A. W., 2002. Garnet-field melting and late-stage refertilization in "residual" abyssal peridotites from the Central Indian Ridge. J. Petrol., 43: 2305-2338.

Hellebrand E. and Snow J.E., 2003. Deep melting and sodic metasomatism underneath the highly oblique-spreading Lena Trough (Artic Ocean). Earth Planet. Sci. Lett., 216: 283-299.

Hilde T.W.C. and Lee C.S., 1984. Origin and evolution of the West Philippine Basin: a new interpretation. Tectonophysics, 102: 85-104.

Hirose K. and Kawamoto T., 1995. Hydrous partial melting of lherzolite at 1 GPa: the effect of H_2O on the genesis of basaltic magmas. Earth Planet. Sci. Lett., 133: 463-473.

Hirschmann M.M. and Stolper E.M., 1996. A possible role for garnet pyroxenite in the origin of the "garnet signature" in MORB. Contrib. Mineral. Petrol., 124: 185-208.

Hirschmann M.M., Asimow P.D., Ghiorso M.S. and Stolper E.M., 1999. Calculation of peridotite partial melting from thermodynamic models of minerals and melts. III. Controls on isobaric melt production and the effect of water on melt production. J. Petrol., 40 (5): 831-851.

Ionov D.A., Savoyant L. and Dupuy C., 1992. Application for the ICP-MS technique to trace element analysis of peridotites and their minerals. Geostand. New., 16: 311-315.

Ionov D.A., Bodinier J.-L., Mukasa S.B. and Zanetti A., 2002. Mechanisms and sources of mantle metasomatism: major and trace element compositions of peridotite xenoliths from Spitsbergen in the context of numerical modelling. J. Petrol., 43: 1-41.

Ishii T., Robinson P.T., Maekawa H. and Fiske R., 1992. Petrological studies of peridotites from diapiric serpentinite seamounts in the Izu-Ogasawara-Mariana forearc, Leg 125. In: P. Fryer, J.A. Pearce, L.B. Stokking et al. (Eds.), Proc O.D.P. Sci Res., 125: 445-486.

Jaques A.L. and Green D.H., 1980. Anhydrous melting of peridotite at 0-15 Kb pressure and the genesis of tholeiitic basalts. Contrib. Mineral. Petrol., 73: 287-310.

Jagoutz E., Palme H., Baddenhausen H., Blum K., Cendales M., Dreibus G., Spettel B., Lorentz V. and Wänke H., 1979. The abundances of major and trace elements in the earth's mantle as derived from primitive ultramafic nodules. Proc. Lunar Planet. Sci. Conf., 10: 2031-2050.

Jochum K.P., Seufert H.M., Spettel B. and Palme H., 1986. The solar system abundances of Nb, Ta and Y, and the relative abundances of refractory lithophile elements in differentiated planetary bodies. Geochim. Cosmochim. Acta, 50: 1173-1183.

Johnson K.T.M., Dick H.J.B. and Shimizu N., 1990. Melting in the oceanic upper mantle: an ion microprobe study of diopside in abyssal peridotites. J. Geophys. Res., 95: 2661-2678.

Johnson K.T.M. and Dick H.J.B., 1992. Open system melting and temporal and spatial variation of peridotite and basalt at the Atlantis II Fracture Zone. J. Geophys. Res., 97: 9219-9241.

Kelemen P.B., Hirth G., Shimizu N., Spiegelman M., and Dick H.J.B., 1997. A review of melt migration processes in the adiabatically upwelling mantle beneath oceanic spreading ridges, Phil. Trans. R. Soc. Lond., A, 355: 283-318.

Kinzler R.J., 1997. Melting of mantle peridotite at pressures approaching the spinel to garnet transition: application to mid-ocean ridge basalt petrogenesis. J. Geophys. Res., 102: 853-874.

Kohut E.J., Stern R.J., Kent A.J.R., Nielsen R.L., Bloomer S.H. and Leybourne M., 2006. Evidence for adiabatic decompression melting in the southern Mariana Arc from high-Mg lavas and melt inclusions. Contrib. Mineral. Petrol., 152: 201-221.

Kushiro I., 1990. Partial melting of mantle wedge and evolution of island arc crust. J. Geophys. Res., 95: 15929-15939.

Macpherson C.G. and Hall R., 2001. Tectonic setting of Eocene boninite magmatism in the Izu-Bonin-Mariana forearc. Earth Planet. Sci. Lett., 186: 215-230.

Maekawa H., Fryer P. and Ozaki M., 1995. Incipient blueschist-facies metamorphism in the active subduction zone beneath the Mariana Forearc. In: B. Taylor and J. Natland (Eds.). Active Margins and Marginal Basins of the Western Pacific. Geophys. Monogr., Am. Geophys. Un., 88: 281-290.

Mevel C., 2003. Serpentinization of abyssal peridotites at mid-ocean ridges. C. R. Geosci., 235: 825-852.

Miyashiro A., Shido F. and Ewing M., 1969. Composition and origin of serpentinites from the Mid-Atlantic-Ridge near 24 and 30°N. Contrib. Mineral. Petrol., 23: 117-127.

Mysen B.O. and Kushiro I., 1977. Compositional variations of coexisting phases with degree of melting of peridotite in the upper mantle. Am. Mineral., 62: 843-865.

Mottl M.J., 1992. Pore waters from serpentine seamounts in the Mariana and lzu-Bonin forearcs, Leg 125: evidence for volatiles from the subducting slab. In: P. Fryer, J.A. Pearce, L.B. Stokking et al. (Eds.), Proc. O.D.P., Sci. Res., 125: 373-385.

Mottl M.J., Komor S.C., Fryer P. and Moyer C.L., 2003. Deep-slab fluids fuel extremophilic Archaea on a Mariana forearc serpentinite mud volcano: Ocean Drilling Program Leg 195. Geochem. Geophys. Geosyst. 4 (11): 9009, doi:10.1029/2003GC000588.

Niu Y., 1997. Mantle melting and melt extraction processes beneath ocean ridges: evidence from abyssal peridotites. J. Petrol., 38 (8): 1047-1074.

Niu Y., O'Hara M. and Pearce J.A., 2003. Initiation of subduction zones as a consequence of lateral compositional buoyancy contrast within the lithosphere: a petrological perspective. J. Petrol., 44 (5): 851-866.

Ohara Y. and Ishii T., 1998. Peridotites from the southern Mariana forearc: heterogeneous fluid supply in mantle wedge. Island Arc, 7: 541-558.

Ozawa K. and Shimizu N., 1995. Open-system melting in the upper mantle: Constraints from the Hayachine-Miyamori ophiolite, northeastern Japan. J. Geophys. Res., 100: 22315-22335.

Parkinson I.J., Pearce J.A., Thirlwall M.F., Johnson K.T.M. and Ingram G., 1992. trace element geochemistry of peridotites from Izu-Bonin-Mariana forearc, Leg 125. In: P. Fryer, J.A. Pearce, L.B. Stokking et al. (Eds.), Proc O.D.P. Sci Res., 125: 487-506.

Parkinson I.J. and Pearce J.A., 1998. Peridotites from Izu-Bonin-Mariana forearc (ODP Leg 125): evidence for mantle melting and melt-mantle interaction in a supra-subduction zone setting. J. Petrol., 39 (9): 1577-1618.

Parkinson I.J. and Arculus R.J., 1999. The redox state of subduction zones: insights from arc-peridotites. Chem. Geol., 160: 409-423.

Pearce J.A., Barker P.F., Edwards S. J., Parkinson I. J. and Leat P.T., 2000. Geochemistry and tectonic significance of peridotites from the South Sandwich arc-basin system, South Atlantic. Contrib. Mineral. Petrol., 139: 36-53.

Piccardo, G.B., Müntener, O., Zanetti, A., Pettke, T., 2004a. Ophiolitic peridotites of the Alpine-Appenine system: mantle processes and geodynamic relevance. Int. Geol. Rev., 46: 1119-1159.

Piccardo G.B., Müntener, O., Zanetti A., Romairone A., Bruzzone S., Poggi E. and Spagnolo G., 2004b. The Lanzo South peridotite: melt/peridotite interaction in the mantle lithosphere of the Jurassic Ligurian Tethys. Ofioliti, 29 (1): 37-62.

Piccardo G.B., Zanetti A., Spagnolo G. and Poggi, E., 2005. Recent researches on melt-rock interaction in the Lanzo South peridotite. Ofioliti, 30 (2): 115-124

Piccardo G.B., Zanetti A., Poggi E., Spagnolo G. and Müntener O., 2006. Melt/peridotite interaction in the Southern Lanzo peridotite: Field, textural and geochemical evidence. Lithos, pp. 29.

Rampone E., Hofmann A.W., Piccardo G.B., Vannucci R., Bottazzi P. and Ottolini L., 1995. Petrology, mineral and isotope geochemistry of the External Liguride peridotites (Northern Apennine, Italy). J. Petrol., 36: 81-105.

Rampone E., Romairone A., Hofmann A., 2004. Contrasting bulk and mineral chemistry in depleted mantle peridotites: evidence for reactive porous flow. Earth Planet. Sci. Lett., 218: 491-506.

Sachan H.K., 2001. Supra-subduction origin of the Nidar ophiolitic sequence, Indus Suture Zone, Ladakh, India: Evidence from mineral chemistry of upper mantle rocks. Ofioliti, 26 (1): 23-32.

Savov I.P, Hickey-Vargas R., D'Antonio M., Ryan J.G. and Spadea P., 2006. Petrology and geochemistry of West Philippine Basin basalts and early Palau-Kyushu volcanic clasts from ODP Leg 195, Site 1201D: implications for the early history of the Izu-Bonin-Mariana arc. J. Petrol., 47: 277-299.

Scambelluri M., Rampone E. and Piccardo G.B., 2001. Fluid and element cycling in subducted serpentinite: a trace element study of the Erro-Tobbio high-pressure ultramafites (Western Alps, NW Italy). J. Petrol., 42: 55-67.

Seyler M., Toplis M., Lorand J.P., Luguet A. and Cannat M., 2001. Clinopyroxene microtextures reveal incompletely extracted melts in abyssal peridotites. Geology, 29: 155-158.

Shaw D.M., 1970. Trace element fractionation during anatexis. Geochim. Cosmochim. Acta, 34: 237-243.

Shipboard Scientific Party, Proceed O.D.P. Init. Rept. 195: 2002, 233 [CD-ROM]. Available from: Ocean Drilling Program, Texas A&M University, College Station TX 77845-9547, USA.

Snow J. E. and Dick H.J.B., 1995. Pervasive magnesium loss by marine weathering of peridotite. Geochim. Cosmochim. Acta, 59: 4219-4235.

Spadea P., Zanetti A. and Vannucci R., 2003. Mineral chemistry of ultramafic massif in the Southern Uralides orogenic belt (Russia) and the petrogenesis of the Lower Paleozoic ophiolites of the Uralian Ocean. In: Y. Dilek and P.T. Robinson (Eds.), Ophiolites in Earth history. Geol. Soc. London Spec. Publ., 218: 567-596.

Suhr G., Seck H.A., Shimizu N., Günther D. and Jenner G., 1998. Infiltration of refractory melts into lowermost oceanic crust: evidence from dunite- and gabbro-hosted clinopyroxenes in the Bay of Islands Ophiolite. Contrib. Mineral. Petrol., 131: 136-154.

Suhr G., 1999. Melt migration under oceanic ridges: inferences from reactive transport modelling of upper mantle hosted dunites. J. Petrol., 40: 575-599.

Suhr G. and Edwards J.E., 2000. Contrasting mantle sequences exposed in the Lewis Hill massif: evidence for early, arc-related history of the Bay of Islands ophiolite. Geol. Soc. of Am. Spec. Paper, 349: 433-442.

Suhr G., Hellebrand E., Snow J.E., Seck H.A. and Hofmann, A.W., 2003. Significance of large, refractory dunite bodies in the upper mantle of the Bay of Islands Ophiolite. Geochem. Geophys. Geosyst. G^3, 4, 2001GC000277.

Takano Y., Kobayashi K., Yamanata T., Marmo K. and Urabe T., 2004. Amino acids in the 308°C deep-sea hydrothermal system of the Suiyo Seamount, Izu-Bonin Arc, Pacific Ocean. Earth Planet. Sci. Lett., 219: 147-153.

Vernières L., Godard M. and Bodinier J.-L., 1997. A plate model for the simulation trace element fractionation during partial melting and magma transport in the Earth's upper mantle. J. Geophys. Res., 102: 24771-24784.

White R.S., 1988. The Earth's crust and lithosphere. J. Petrol., Special Lithosphere Issue, p. 1-10.

Zanetti A., Vannucci R., Bottazzi P., Oberti R. and Ottolini, L., 1996. Infiltration metasomatism at Lherz as monitored by systematic ion-microprobe investigations close to a hornblendite vein. Chem. Geol., 134: 113-133.

Zhou M.-F., Robinson P.T., Malpas J., Edwards S.J. and Qi L., 2005. REE and PGE geochemical constraints on the formation of dunites in the Luobosa Ophiolite, Southern Tibet. J. Petrol., 46: 615-639.

Received, August 21, 2006
Accepted, November 28, 2006